Nano Research
DOI 10.1007/s12274-014-0645-2
Research Article
ISSN 1998-0124
CN 11-5974/O4

Enabling practical electrocatalyst-assisted photoelectrochemical water splitting with earth abundant materials

Xiaogang Yang[1](✉), Rui Liu[2,3], Yumin He[3], James Thorne[3], Zhi Zheng[1] and Dunwei Wang[3](✉)

Nano Res., **Just Accepted Manuscript** • DOI: 10.1007/s12274-014-0645-2
http://www.thenanoresearch.com on November 19 2014

Just Accepted

TSINGHUA UNIVERSITY PRESS Springer

TABLE OF CONTENTS (TOC)

Enabling practical electrocatalyst-assisted photoelectrochemical water splitting with earth abundant materials

Xiaogang Yang[1]*, Rui Liu[2,3], Yumin He[3], James Thorne[3], Zhi Zheng[1] and Dunwei Wang[3*]

1. Key Laboratory of Micro-Nano Materials for Energy Storage and Conversion of Henan Province and Institute of Surface Micro and Nano Materials, Xuchang University, Henan 461000, China.
2. Joint Center for Artificial Photosynthesis, California Institute of Technology, Division of Chemistry and Chemical Engineering, Pasadena, CA 91125, USA
3. Department of Chemistry, Boston College, Merkert Chemistry Center, 2609 Beacon St., Chestnut Hill, MA 02467 USA

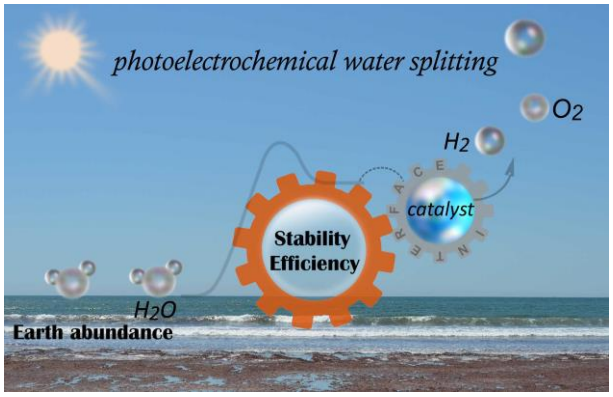

High efficient photoelectrochemical water splitting devices rely on the development of the new earth abundant semiconductors, electrocatalysts, and especially the interfaces between different components.

Provide the authors' webside if possible.

Dunwei Wang, https://www2.bc.edu/dunwei-wang/Research.html

Nano Research
DOI (automatically inserted by the publisher)
Review Article
ISSN 1998-0124
CN 11-5974/O4

Enabling practical electrocatalyst-assisted photoelectrochemical water splitting with earth abundant materials

Xiaogang Yang[1](✉), Rui Liu[2,3], Yumin He[3], James Thorne[3], Zhi Zheng[1] and Dunwei Wang[3](✉)

1. Key Laboratory of Micro-Nano Materials for Energy Storage and Conversion of Henan Province and Institute of Surface Micro and Nano Materials, Xuchang University, Henan 461000, China.
2. Joint Center for Artificial Photosynthesis, California Institute of Technology, Division of Chemistry and Chemical Engineering, Pasadena, CA 91125, USA
3. Department of Chemistry, Boston College, Merkert Chemistry Center, 2609 Beacon St., Chestnut Hill, MA 02467 USA

Received: day month year
Revised: day month year
Accepted: day month year (automatically inserted by the publisher)

KEYWORDS
photoelectrochemical
water splitting,
efficiency,
stability,
interface,
earth abundance

ABSTRACT

Sustainable development and continued prosperity of humanity hinge on the availability of renewable energy sources on a terawatts scale. In the long run, solar energy is the only source that can meet this daunting demand. Widespread utilization of solar energy faces challenges as a result of its diffusive (hence low energy density) and intermittent natures. How to effectively harvest, concentrate, store and redistribute solar energy constitutes a fundamental challenge that the scientific community needs to address. Photoelectrochemical (PEC) water splitting is a process that can directly convert solar energy into chemical energy and store it in chemical bonds, by producing hydrogen as a clean fuel source. It has received significant research attention lately. Here we provide a concise review on the key issues encountered in carrying out PEC water splitting. Our focus is on the balance of considerations such as stability, earth abundance, and efficiency. Particular attention is paid to the combination of photoelectrodes with electrocatalysts, especially on the interfaces between different components.

1. Introduction

The primary source of energy supply for the rapidly growing global economy is fossil fuels. They are nonrenewable and being depleted at an ever increasing pace [1]. Combining this concern with the devastating environmental impact caused by burning fossil fuels, we see an urgent need for the development of large scale solar energy harvesting and storage technologies. Among the approaches under study, including station batteries and pumped hydroelectricity, technologies that can

Address correspondence to Xiaogang Yang, xiaogang.yang@gmail.com; Dunwei Wang, dunwei.wang@bc.edu

directly utilize the harvested solar energy to power thermodynamically uphill reactions are attractive because they offer a simple route to simultaneous solar energy conversion and storage. In addition, the resulting chemicals can be used as fuels, which can be concentrated and redistributed using existing infrastructures. Indeed, significant research interest has been attracted to advance processes that are commonly referred to as artificial photosynthesis as they are similar to natural photosynthesis in how energy is harvested and used to drive chemical reactions [2]. While a variety of reduction chemistries, including direct proton reduction for hydrogen generation and CO_2 reduction for hydrocarbons, are concurrently studied, the need for water splitting is recognized as an important first step for photosynthesis [3]. The importance of water splitting in natural photosynthesis is well understood. It extracts, excites, and transports electrons away from water oxidation sites for eventual usage in dark reactions for CO_2 reduction. Thermodynamically, the energy gain in photosynthesis is complete during the step of water splitting; the following reduction steps are but a storage solution. Within this context, we understand that the importance of water splitting to solar fuel production goes beyond hydrogen generation [4]. In order to successful split water using sunlight as one (and ultimately the only) energy input, we need a mechanism to absorb sunlight, use the energy to separate charges, and catalyze redox reactions. Of the studied routes for this purpose, photoelectrochemical (PEC) reactions represent one of the most promising approaches because they hold promise for high efficiency, low cost and long durability [5]. First reported in 1968 [6] but popularized by Honda and Fujishima in 1972 [7], the concept was initially demonstrated on TiO_2. Many researches followed their work during the next four decades. The continuous efforts notwithstanding, progress in the field has been sluggish. While high efficiencies have been reported, these proof-of-concepts were based on high-cost (either due to scarcity of their composition elements or due to complexities in their fabrication) materials [8, 9]. In addition, photocorrosion of these materials raise serious questions about their practicality for long-term usages. It is noted that recently significant advances have been made to stabilize high-efficiency photoelectrodes [10, 11]. Alternatively, earth-abundant (and hence, low-cost) materials those are stable against photocorrosion typically suffer low efficiencies. The intention of this review article is to examine issues that plague research on earth-abundant materials. We present an overview of recent progress of this field and provide our perspective on how the field can be advanced, by highlighting issues we believe are key to further development.

On a fundamental level, the behaviors of a photoelectrode in a PEC system are described by two well-developed mathematical expressions. The first one governs the diode behavior of the semiconductor (Schottky equation) [12], and the second one determines the catalytic behavior on the surface (Bulter-Volmer equation) [13-15]. However, important distinctions need to be made here. The true "PEC" behavior of a photoelectrode tends to be more complex than a simple combination of a photovoltaic (PV) component and an electrolyzer [16]. This is because the semiconductor/liquid junction (interface) in a PEC system influences both the diode and the catalytic behaviors at the same time. New sciences are necessary to fully understand the intricacies. By comparison, a PV plus electrolyzer configuration relies on solid-state junctions for charge separation. Its optimization is essentially an engineering challenge, one centering around how to lower the cost and increase the stability. This review article primarily deals with photoelectrodes in a PEC system.

A typical PEC water splitting cell consists of three critical components: at least one semiconductor to absorb light and separate charge (as photoabsorber), counter electrode and electrolyte [5]. Hydrogen can be produced/stored through the water splitting process: $H_2O(l) \rightarrow H_2(g)+1/2O_2(g)$, by conversion of solar energy to chemical energy (ΔG° = 237.1 kJ/mol, corresponding to ΔE° = 1.23 V per electron) [17]. Compared with the photovoltaic-driven electrochemical water

electrolysis, the PEC water splitting devices exhibit potential advantages of low cost [18, 19]. As far as efficiencies are concerned, a PEC photoelectrode would perform almost identical to a photovoltaic system based on calculations performed in 1980's by Bolton et al. [20] using detailed thermodynamic balances. It was shown that the PEC system can be as efficient as a photovoltaic system under a minimum overpotential of 0.38 V. The minimum overpotential is a result of the difference between the internal energy (bandgap of the semiconductor) and the free energy (1.23 V needed for water splitting per electron). Recently, there are renewed interests in similar calculations, with new information concerning various device-engineering considerations added to the system. For instance, a calculation by Seitz et al. [21] showed that the highest solar-to-hydrogen (STH) efficiencies can reach 11.2 %, 22.8% and 15.5 % on a single absorber (Eg = 2.26 eV), dual stacked absorbers (Eg = 1.84 and 1.23 eV) and dual side-by-side absorbers (Eg = 1.59 eV), respectively. Based on calculations similar to Bolton's, Lewis et al., the impact of kinetic overpotentials on the overall efficiencies of dual absorber systems have been evaluated, by assuming continuous adjustment of the band gap and band edge positions of the semiconductors. Their conclusion was that the overall efficiencies are more sensitive to the band gaps of the semiconductor than to the kinetic overpotentials [14]. Experimentally, the STH efficiencies can be obtained on a true system in a two-electrode configuration as Equation (1) [5]:

$$\eta_{\mathrm{STF}} = \frac{J_{\mathrm{SC}} \times (1.23\ \mathrm{V})}{P_{\mathrm{IN}}} \qquad (1)$$

where J_{SC} is the maximum current for the complete cell with zero bias as short circuit current density, P_{IN} is the overall photon energy flux input into the device (e.g. for simulated solar light AM 1.5G, 100 mW/cm^2). In this equation, a 100% Faradaic efficiency for hydrogen evolution reaction (HER) and oxygen evolution reaction (OER) is assumed on each electrode. To achieve such ideal Faradaic efficiencies, we need high-performance catalysts. When an external applied bias is needed for the complete water splitting in two electrode configuration, the applied bias photon-to-current efficiency (ABPE) has also been suggested to evaluate PEC performance of photoelectrodes [22].

To separately assess the properties of individual photoelectrodes, three-electrode configuration is often employed to study PEC systems. This configuration is advantageous because when a reference electrode is present, the potential of the working photoelectrode can be accurately measured, which provides an estimate of how much electrical energy is put into the working electrode. What is obtained is that power conversion efficiencies of a photoelectrode based on the half reaction of water splitting. Under such conditions, the steady-state current-voltage curves can be treated as a typical current-voltage curve of a photovoltaic device. Thus, the onset potential (V_{on}) and short circuit current density (J_{SC}) at the referenced thermodynamic potential of water splitting reaction ($E_{\mathrm{H^+/H_2}}$, $E_{\mathrm{O_2/H_2O}}$) can be applied to evaluate the PEC performance. The power converting efficiency (η) of the photocathode can be calculated (in Equation 2) from the current density-potential *J-V* curves, where J is the maximum photocurrent (in mA/cm^2) at the maximum power point, P_{IN} is the power (in mW/cm^2) of the illumination input into the system:

$$\eta_{\mathrm{photocathode}} = \frac{\left| J \times (V_{\mathrm{bias}} - E_{\mathrm{H^+/H_2}}) \right|_{\mathrm{mp}}}{P_{\mathrm{IN}}} \qquad (2)$$

For a photoanode, the power conversion efficiency can be similarly calculated based on the *J-V* data, where the ($E_{\mathrm{O_2/H_2O}} - V_{\mathrm{bias}}$) was used:

$$\eta_{\mathrm{photoanode}} = \frac{\left| J \times (E_{\mathrm{O_2/H_2O}} - V_{\mathrm{bias}}) \right|_{\mathrm{mp}}}{P_{\mathrm{IN}}} \qquad (3)$$

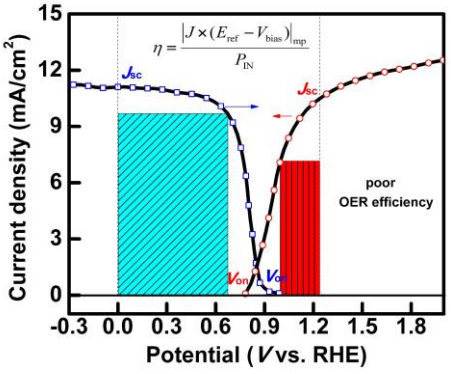

Figure 1. Current density- potential behavior for a photoanode and photocathode with external applied bias versus reversible hydrogen electrode (RHE) in three electrode configuration. The cyan shadow represents the maximum power conversion efficiency of a photocathode, while the red shadow represents the maximum power conversion efficiency of a photoanode.

It is critical to note here that the evaluation of photoelectrode efficiencies by Equations (2) and (3) should be carried out with extreme cautions. Strictly speaking, they are only meaningful when no additional energy is supplied to the counter electrode for the other half reactions, a condition that is rarely met, if at all. It has been shown by Grimes et al. that three-electrode methods often lead to overestimate of efficiencies [23]. These two equations are of value only when used to compare performance of various photoelectrodes. Based on these considerations, Figure 1 is generated by evaluating photoanode and photocathode separately. We see from Figure 1 that when unassisted water splitting does happen, the current density at the point where the *J-V* curves intersect is the only parameter that matters in defining the maximum overall efficiency. It is therefore important to shift the two curves so that the intersecting point is close to the maximum power point of each individual *J-V* curve. It means that the combined V_{on}'s, voltage at which photocurrent is first measured, or the sum of photovoltages should be greater than 1.23 V. In addition to increasing charge collection efficiency, which translates to how "square" each individual *J-V* curve is, as measured by fill factors, we desire to have high photovoltages (V_{ph}), as measured by the difference between the corresponding electrochemical potential of the redox reaction and V_{on}, V_{ph}=1.23 V- V_{on} for photoanode, and V_{ph}=V_{on} for photocathode. Currently, the practical STH efficiencies are much lower than the theoretical values, due to this mismatch of the *J-V* curves of the photoanode and photocathode.

It is now broadly agreed upon that a single material will unlikely meet all the requirements simultaneously to deliver high STH efficiencies. These requirements include good light absorption (within the solar spectrum), suitable conduction and valence band edge driving the water reduction and oxidation reactions, rapid charge transfer, low cost, and high stability. How to independently tailor material's properties in each aspect is a daunting challenge. What makes it even more challenging is that the complex interplays between various aspects of the properties. For example, even though the FeOOH is a modest OER catalyst, it showed a synergetic electrocatalytic performance when interfaced with the $BiVO_4$ photoanode by the photoelectrodeposition [24]. The cobalt phosphate (Co-Pi) is regarded as an efficient OER catalyst, which dramatically reduced the OER overpotential and suppress the electron-hole recombination on Fe_2O_3 [25] and $BiVO_4$ [26] photoanodes, showing a cathodic shift of the V_{on}. However, the function of these Co-Pi catalyst on the semiconductor has not been well agreed upon. For instance, the "Co-Pi" catalyst resulted in an alternation of the charge transport pathway and enhanced charge transfer kinetics for water splitting, where a Schottky-type heterojunction was formed to reduce the recombination loss, as proposed by Barroso et al. [27]. The catalytic layer can store photogenerated holes from the semiconductor and further oxidation water to form oxygen molecules. An opposing argument by other groups is that the "catalytic" layer as a spectator only increase the concentration of minority charges in the semiconductor by a passivation of charge recombination [28]. Works based on Al_2O_3, Ga_2O_3, In_2O_3, and TiO_2 non-catalyst on hematite has been treated as a surface

passivation layers, which reduce surface charge recombination [29-31]. Some electrocatalysts reduce holes concentration in Ta-base semiconductor, showing both enhanced PEC efficiency and improved stability [32]. These apparently conflicting results highlight the intricacy of a PEC system and point out the importance of semiconductor|electrocatalyst interface to the overall performance [33, 34].

Although direct application of electrocatalysts onto highly engineered tandem or triple-junction photovoltaic architectures has been demonstrated [35], there remains a need for direct combinations of catalysts with a simple semiconducting photoelectrode because such a system holds the potential of low cost. Importantly, to rival natural photosynthesis in scales, we need to study how to construct such simple systems based on earth abundant materials. Jaramillo and coworkers had analyzed the availability for the scarcity of the elements [36]. Additionally, long-term stability of the integrated systems is another important concern. There are several comprehensive reviews on this topic that were published recently [5, 37]; some more focused discussions on how nanostructures [38, 39]; or passivation [40] can influence PEC water splitting performance. In this review, we aim to provide an overview on how earth abundant materials may contribute to the construction of practical PEC water splitting devices, including earth-abundant semiconductor materials, HER and OER catalysts. Special attention is paid to the semiconductor|electrocatalyst interface of systems made of earth-abundant materials.

2. Earth abundant semiconductors

As a key component in the PEC water splitting devices, the semiconducting photoelectrode absorbs solar light and separates charge in the space charge region. This charge separation function requires a built-in field that is a result of Schottky-type diode formed at the solid-liquid junction (interface). Earth abundant materials used in water splitting need to have suitable band gap to absorb light in the visible range; it should also generate large enough photovoltages to power water splitting; charge transport must be effective, as well. Earth abundant materials such as Si [41], TiO_2 [42, 43], Fe_2O_3 [44], WO_3 [45], $BiVO_4$ [46], $TiSrO_3$, ZnO, Cu_2O, CuO, SiC etc. have been extensively studied [37]. These materials typically suffer low STH efficiencies for various reasons, with poor charge transport on the top of the list. How to improve their STH efficiencies is a main challenge faced by this field.

There are several strategies for the improvement of the water splitting performance. 1) Nanostructuring is believed to be able to increase surface area for better light absorption, to improve charge separation, and to enhance charge transportation. For example, nanostructured morphology is expected to improve the performance of hematite significantly, which is of a desired band gap (Eg=2.1 eV) but with notoriously short minority carrier diffusion lengths [47-50]. The Grätzel group reported that cauliflower-like hematite nanostructures prepared by atmosphere pressure chemical vapor deposition (APCVD) showed significantly improved photocurrent as compared to other hematite structures [51]. Similarly, photoelectrodes such as TiO_2 [42], WO_3 [52], $TiSrO_3$ [53], ZnO [54], Ta_3N_5 [55] used in solar water splitting have all been reported to perform better when manufactured into nanostructures. 2) Doping is expected to increase carrier density and, thus, enables better charge transport. For instance, Li et al. reported photocurrent density of 1.86 mA/cm^2 at 1.23 V vs RHE on Sn-doped nanostructured hematite photoanode [56]. In addition, doped semiconductors are commonly shown to perform better than their counterparts without intentional doping. Examples can be found in $BiVO_4$ [57-60], WO_3 [61-63], ZnO [54, 64-67], Fe_2O_3 [68-72], among others. Another approach of using dopants is to broaden light absorption as dopants may introduce mid-gap states. Examples include of the application of N, S, C, B, P, Ag, Fe, V, Au and Pt in TiO_2 for visible light absorption [42, 43, 73, 74]. It is cautioned, however, that results in this direction are often challenged, and more convincing experimental results are needed to further prove the

claimed effects. 3) Introduction of additional materials components dedicated for charge transport or charge separation or both has been attempted as well. By depositing hematite onto Si nanowires as photoanode, for example, Mayer et al. demonstrated a dual absorber system with onset potential close to 0.6 V (vs. RHE) in 1.0 M KOH aqueous solution [75]. Atwater and Lewis et al. reported WO_3|Si microwire structures for water splitting which could operate in acidic condition [76, 77]. Similarly, TiO_2|Si heterojunction [78], $BiVO_4$|Si heterojunction [79], $LaTiO_2N$|In_2O_3 heterojunction [80], $CuBi_2O_4$|CuO heterojunction [81] and InGaN|GaN heterojunction [82] have been investigated by different groups, confirming the validation of the dual-absorber configuration.

Presently, the most studied earth-abundant semiconductors for PEC water splitting include crystalline silicon (c-Si), amorphous silicon (a-Si), Cu_2O, Fe_2O_3, $BiVO_4$ and WO_3. For future applications, the stability against photocorrosion of Si-based photoelectrodes needs to be improved dramatically. This is especially true when it is used as a photoanode. The fabrication cost of Si needs to be reduced significantly, as well. For Fe_2O_3 and $BiVO_4$ as photoanode, their onset potentials (V_{on}) need to be largely shifted toward the cathodic direction. Their photocurrent also needs significant enhancement. As for WO_3, better stability in neutral or alkaline solution is desired. Broader light absorption in the visible range is required, as well.

In the meantime, researchers are working hard to find new compounds based on earth-abundant elements for PEC water splitting applications. For example, metal sulfides also can be applied as photoelectrodes for water splitting. Yokoyama et al.[83] have prepared Cu_2ZnSnS_4 (CZTS, Eg=1.5 eV) thin films as photocathode by co-sputtering techniques, which exhibited a solar energy conversion efficiency to H_2 production of 1.2% by surface modification with Pt, CdS, and TiO_2. Sun et al. reported that all-surface-atomic SnS (or SnSe) two-dimensional (2D) nanosheets fabricated through an ultrasonic strategy can be used for this purpose [84]. Electronic structures of the single layer structure of nitride halide MNX (M=Ti, Zr, Hf, X=Cl, Br, I) had been studied by Liu et al. [85]. Some of these materials are expected to exhibit suitable band gaps (2.23-2.83 eV) and may be promising candidates for water splitting. Li et al. have used density functional theory (DFT) to predict band gaps and electronic structures of metal oxides, chalcogenides, nitrides in doped layered structure [86]. In Bartlett's group, $CuWO_4$ (Eg=2.25 eV) [87] was found as a n-type semiconductor, which can be made into photoanode with nearly quantitive Faradaic efficiency for water oxidation reaction. Masashi et al. have prepared p-type SiC by epitaxial growth and used it as a photocathode. The resulting photoelectrode enabled self-driven water splitting with an STH efficiency of 0.38% [88]. Baeg et al. have prepared W-doped $FeVO_4$ (Eg=2.06 eV) using layer-by-layer deposition of metal-organic precursor and subsequent thermal decomposition at 550 °C in air. A photon to current conversion efficiency of 6.5% illuminated at 400 nm was observed [89]. BiOX (X=Cl, Br, I) has been extensively studied by Zhang and his coworkers as photocatalysts for water splitting [90]. Hahn et al. reported a pyrolysis synthesis of n-type BiOI nanoplatelet films as photoelectrodes at various temperatures, which showed photocurrent of 0.9 mA/cm^2 at 0.4 V (vs. Ag/AgCl) in acetonitride by oxidation of I^- to I_3^- [91]. Carbon nitride (C_3N_4, Eg=2.7 eV) was found as a promising semiconductor made of earth abundant elements for slurry-based solar water splitting [92].

Besides meeting the earth abundance requirement, an ideal material used for water splitting must also be stable in aqueous solutions for practical PEC water splitting applications. Even if a material exhibits reasonable stability when used as an individual photoelectrode, the stability needs to be studied carefully when in an integrated system under harsh conditions (strong illumination, extremely high or low pH's). According to the work by Wang et al. [93] in Figure 2, photoanode materials are unstable when the material's oxidation

potential, ϕ^{ox}, is more negative than the oxygen evolution potential, $E(O_2/H_2O)$. When ϕ^{ox} is positive of the valence band maximum (VBM), the material is thermodynamically stable. When $E(O_2/H_2O) < \phi^{ox} < E_{VBM}$, the stability of a material depends on the relative rate of consumption of holes for water oxidation vs surface corrosion. Similar arguments on photocathode condition can be made.

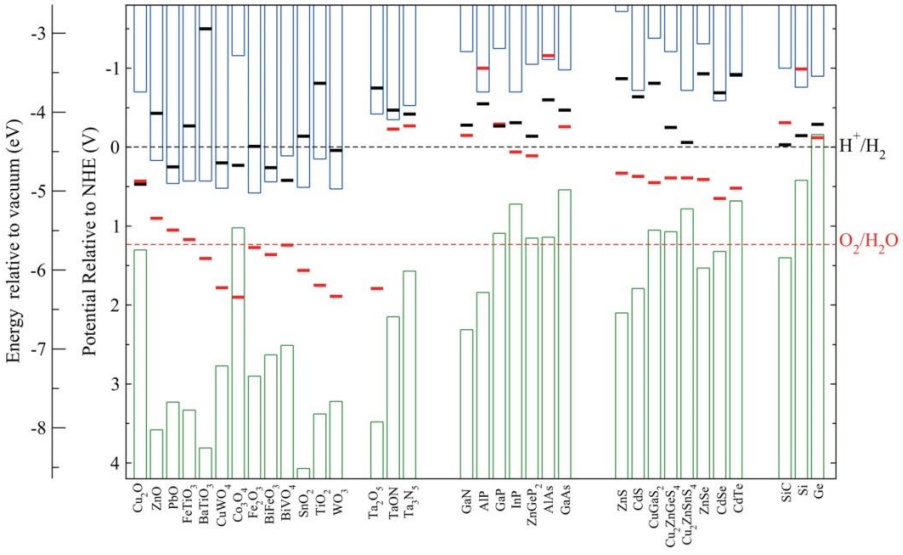

Figure 2. Calculated oxidation potential ϕ^{ox} (red bars) and reduction potential ϕ^{re} (black bars) relative to the NHE and vacuum level for a series of semiconductors in solution at pH = 0, the ambient temperature 298.15 K, and pressure 1 bar. The water redox potentials $E(O_2/H_2O)$ and $E(H^+/H_2)$ (dashed lines) and the valence (green columns) and conduction (blue columns) band edge positions at pH = 0 are also plotted. Reprinted with permission from Ref. [93], Copyright (2012) American Chemical Society.

Recently a review paper by Liu et al. discussed the details on how the surface layer could protect the unstable photoelectrodes [40]. When a surface passivation layer is used, oxidation potential of the surface layer material will be more positive than the VBM of the underlying photoabsorber material. For the case of a photocathode protection, the reduction potential of surface protection layer has to be more negative than the conduction band minimum (CBM) of photoabsorber.

Experimentally, a conformal TiO_2 layer has often been used as a surface passivation layer (in Figure 3). For instance, in 2011, Chen et al. has prepared a 2 nm thin TiO_2 layer on n-Si by ALD, showing that the photocorrosion of silicon can be significantly suppressed [94]. Seger et al. demonstrated that with a sputtered 100 nm TiO_2 layer, p-Si can be protected from water reduction [95]. Hu et al. also reported a 100 nm TiO_2 overlayer on n-Si deposited by ALD would prevent n-Si from photocorrosion and achieve at least 24 hours stability [11]. In both cases, the thick TiO_2 layer showed good conductivity for the light generated carriers to transfer from semiconductor to the electrolyte. More work such as $TiO_2|Nb_2O_5$ protected GaP for water reduction, TiO_2 protected p-Cu_2O for water reduction or graphene protected n-Si for water oxidation are reported based on the same protection concept. By applying these surface protection layers, researchers can play with the small band gap, unstable semiconductors for water splitting, such as GaAs, GaP, CdTe, Cu_2O, and InP. For similar reasons, other metal oxides, such as $CuWO_4$, Co_3O_4, SnO_2, WO_3, Ta_2O_5 etc., may serve as a passivation layer for photoanodes, while $BaTiO_3$ and Ta_2O_5 could be used on photocathodes.

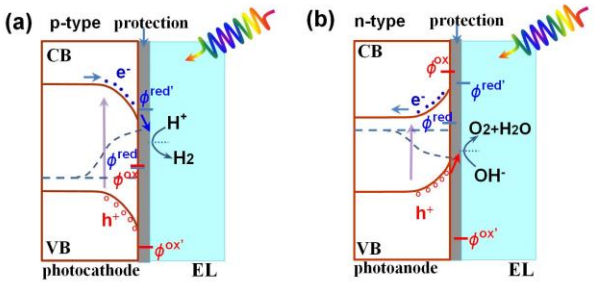

Figure 3. Thermodynamically protection of the unstable photoelectrode by a dense conformal passivation layer under illumination in aqueous electrolyte (EL): (a) cathodic protection of p-type photocathode (e.g. Cu_2O) by stable wide bandgap materials (e.g. TiO_2) in acidic solution; (b) anodic protection of n-type photoanode (e.g. n-Si) by stable wide bandgap materials (e.g. TiO_2) in alkaline solution. ϕ^{red} and ϕ^{ox} are the corrosion potentials of semiconductor due to reduction and oxidation, respectively. $\phi^{red'}$ and $\phi^{ox'}$ are the corrosion potentials of the protection layer due to reduction and oxidation, respectively.

However, the surface passivation layer has its limitations. For instance, a conformal dense layer is often necessary for effective protection; the thick layer, however, may hijack the water|semiconductor interface with a new catalyst|semiconductor one that completely changes the band diagram of a PEC photoelectrode. To be better or worse, PEC performance may result from the new interface. Charge transfer kinetics across the protection layer is of critical importance as well. The general consensus is that OER and HER co-catalysts are needed for high performance PEC water splitting. We next summarize results in this front.

3. Hydrogen evolution reaction

Since electrocatalysts are regarded as promoters for hydrogen evolution reactions on the photocathode, direct incorporation of electrocatalysts onto photoabsorbers introduces new interfaces or junctions. The PEC performance of the photocathode, in terms of power conversion efficiencies and photostability, may be significantly influenced as a result. To the first order approximation, the role of the catalyst is to reduce reaction overpotentials. In a simplified model, the semiconductor absorbs light and separates photogenerated charges; the charges then pass through the electrocatalysts for HER (or OER). The presence of HER electrocatalyst on a photocathode is expected to maximize V_{on} and, hence, the overall STH efficiencies (η).

For integration with p-type semiconductors, earth abundant HER electrocatalysts that exhibit high efficiency, high stability and low light absorption are most favored. For example, NiO, MoS_2 [96, 97], Mo_3O_4, MoS_3 [98], RuO_2, Ni_2P [99], $Ni_{12}P_5$, Ni, Ni-Mo [100], WS_2, WS_3 have been recently studied for HER [41]. Interestingly, amorphous forms of these catalysts often exhibit higher HER performance, presumably due to increased active site densities. For further reading on these earth-abundant inorganic HER catalysts, the readers are referred to a recent review paper by Feber et al. [38]. In the next part, we focus on the electrocatalyst-assisted *photo*electrochemical water reduction. Both power conversion efficiencies and stability of these materials will be considered. What is left out is verification of hydrogen production and the corresponding Faradaic efficiencies as these important issues are often not adequately addressed in the literature.

3.1 Pt catalyst assisted HER

Although Pt based HER catalysts are not earth abundant, they enable the highest HER activity [101]. As such, they have been applied to earth-abundant photocathodes to show highly encouraging results. For example, Boettcher et al. have prepared discontinuous Pt film (1.5 nm) coated n^+p-Si film, which showed high photocurrent at about 28 mA/cm^2 (at 0 V vs. RHE) and ca. 9.6% power efficiency under 100 mW/cm^2 ELH illumination [102]. For n^+p-Si microwires (SiMWs) synthesized by Cu catalyzed chemical vapor deposition (CVD), they also found that the photocurrent decreased to 15 mA/cm^2 and the open circuit voltage slightly decreased to 0.54 V, resulting in a 5.8% of power conversion efficiency.

The SiMWs photocathodes were stable in 0.5 M K_2SO_4 (pH = 2) for 22 h during the PEC measurement, with the fill factor decreased from 0.67 to 0.62. Dasgupta et al. [103] have modified p-Si nanowires (NWs) arrays by Pt nanoparticles (0.5-3 nm) through atomic layer deposition (ALD), the p-SiNWs | Pt enabled photocurrents as high as 20.7 mA/cm^2 and a moderate onset potential (V_{on}) at about 0.25 V, corresponding to power conversion efficiencies at about 1.3%. The Si NWs surface can be protected by 10-12 nm TiO_2 layer from the oxidation of the surface in 0.5 M H_2SO_4 solution. Dai et al. has compared the PEC performance of p-Si nanowires decorated with Pt nanoparticle by ALD and electroless-deposited (ELD) in 0.5 M Na_2SO_4-H_2SO_4 solution (pH=1), showing that a higher V_{on} was obtained on uniform decorated Pt by ALD than that on top-end decoration with ELD Pt [104]. Although the photocurrent and the power conversion efficiency of p-SiNWs | Pt(ALD) photoelectrode was slightly lower than that on p-SiNWs | Pt(ELD), the stability of p-SiNWs by ALD Pt exhibited negligible degradation. Kye et al. used Pt monolayer on p-Si by underpotential deposition of Cu and galvanic exchange, achieving a photocurrent of ca. 17.5 mA/cm^2 and a V_{on} of 0.25 V [105].

Pt-enhanced solar water splitting has been also successfully demonstrated on other semiconductors. Paracchino and co-workers deposited Al doped zinc oxide (AZO) and TiO_2 bilayers between the Cu_2O (Eg=2.0 eV) and Pt electrocatalyst (in Figure 4). The resulting photocathode showed a short circuit current of 5.7 mA/cm^2 and an improved efficiency of 0.57% [106]. The photocathode was stable in 1 M Na_2SO_4-0.1 M potassium phosphate solution (pH=4.9), with 22% photocurrent decay in 20 min. Similar results have been recently obtained by Dai et al. [107] as well, although their approach focused on improving photovoltage instead of photocurrents. Kim and coworkers prepared $CuGaSe_2$ films (1-1.2 μm, by vacuum co-evaporation) with Pt decoration as a photocathode, where a photocurrent of ca. 4.8 mA/cm^2 and an onset potential of 1.1 V in 0.1 M Na_2SO_4 (pH=9.5 adjusted by NaOH) were achieved [108]. The corresponding power conversion efficiency was ca. 0.35%. However, the optimized Ga/Cu ratio was found to be 3~3.5, which may increase the device cost. Gunawan et al. prepared p-n junction of $CuInS_2$ coated with In_2S_3 layer followed by loading of Pt as an efficient hydrogen evolution photocathode and achieved a maximum power conversation efficiency of 2% at 0.28 V in 0.1 M Na_2SO_4 (pH=9), where the photocurrent of 15 mA/cm^2 at 0 V and an onset potential of 0.78 V were observed [109]. It is worth noting that transition metal dichalcogenides (ME_2, where M is Mo or W, E is S or Se) with layered structures have bandgaps ranging from 1.09~1.35 eV, offering potentially high theoretical STH efficiencies and correspond to the saturated photocurrents up to 44.4 mA/cm^2 [86]. Indeed, Pt or Pd decorated p-WS_2 single crystals as photocathodes showed similar hydrogen evolution efficiencies (7%) in 9 M H_2SO_4 solution as reported by Baglio et al. early in 1983 [110]. Nevertheless, high quality single crystals of chalcogenides are often expensive to fabricate.

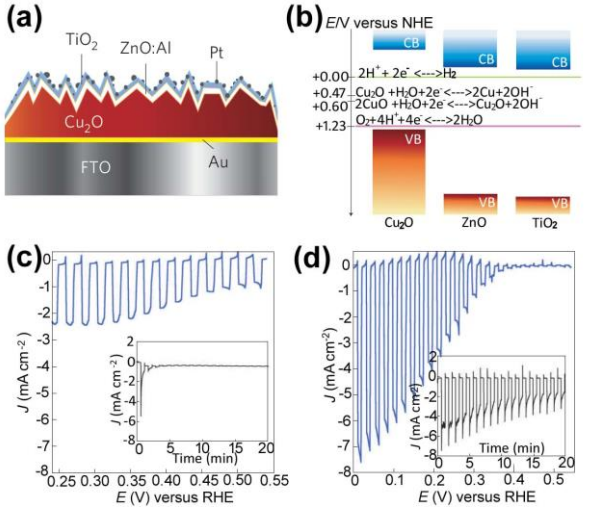

Figure 4. High active p-Cu_2O photocathode protected with AZO and TiO_2 interlayers and Pt HER catalyst, adapted from Nature Materials [106], reprinted by permission from Macmillan Publishers Ltd, Copyright (2011): (a) Schematic

representation of the structure of the surface-protected Cu_2O electrode. (b) Overview of the energy band positions for the semiconductors of the multilayer photocathode and redox levels of the involved chemical reactions. (c) The photoelectrochemical response *J-V* curves for the bare electrode in 1 M Na_2SO_4 solution, under chopped AM1.5 light illumination for the bare Cu_2O electrode. (d) *J-V* curves of the surface protected Cu_2O photocathode, where Cu_2O/5×(4 nm ZnO/0.17 nm Al_2O_3)/11 nm TiO_2 | Pt is used as electrode. The insets show the respective photocurrent transients for the electrodes held at 0 V (vs. RHE) in chopped light illumination with N_2 purging in (c) and (d).

3.2 Earth abundant catalysts assisted HER

Giving the scarcity of Pt, researchers are racing to develop alternatives based on earth-abundant elements. Similar work has been reported by using Si photocathode as a model platform. For example, power conversion efficiencies of these earth-abundant catalyst-decorated Si photocathode ranged between 1.2% and 7.6%, comparable to Si | Pt photoelectrodes (1.3~5.8%) [111-116]. Higher conversion efficiencies could be achieved on n^+p junction of c-Si or p-i-n junction of a-Si, due to the higher photovoltage generated from the enhanced charge separation. Recently, Seger et al. have deposited Ti protection layer and MoS_x electrocatalyst on n^+p Si films, which showed an impressive photocurrent of 16.3 mA/cm² [116]. Lin et al. introduced Ni-Mo electrocatalyst on a-Si (p-i-n junction) protected by TiO_2 layer (80 nm) as a photocathode, on which a higher onset potential of 0.87 V and 11.12 mA/cm² of photocurrent were measured [114]. As far as the stability is concerned, earth abundant catalysts often show poorer performance (some requiring Ti or TiO_2 protection) than Pt. In 1 M $HClO_4$ solution, a p-Si | Mo_3S_4 pillars photocathode decayed 5% in the first 0.5 h [111], while a n^+p Si | Ti | MoS_x photocathode showed stable photocurrent with ~7% decay for 1 h PEC measurement [116]. By and large, the photocorrosion of Si is not serious in acids, making it a good platform for the search of efficient earth abundant HER catalysts.

The knowledge learned on application of earth-abundant HER catalysts on Si can be readily transferred to non-Si photocathodes. For example, Cu_2O based photocathode showed high photovoltage (0.4~0.55 V) and photocurrent (5~5.7 mA/cm² at 0 V vs. RHE) with MoS_x as a catalyst [106, 117, 118]. As shown in Figure 5, Morales-Guio et al. [118] presented a facile ALD method to prepare molybdenum sulfide conformal film (50~100 nm) as a HER catalyst on Cu_2O films (in Figure 5 a to c) which were already protected by an 20 nm AZO and a 100 nm TiO_2 films. The achieved Cu_2O | TiO_2 | MoS_x showed a power conversion efficiency of 0.85%. Notably, the stability of the photocathode improved with the use of TiO_2 passivation and MoS_{2+x} as HER catalyst, corresponding to 50% decay for 5 h in 0.1 M H_2SO_4 (pH=1) solution (in Figure 5d). A nearly 100% of Faradaic efficiency was measured (in Figure 5e). Similar conclusions have been obtained by other groups [107, 119]. Most recently, Dai et al. [107] found that thin ZnS decoration can increase the photovoltage of Cu_2O photocathode to 0.72 V. Notably, they used earth abundant NiMo and CoMo as HER catalysts in PEC water splitting demonstrations.

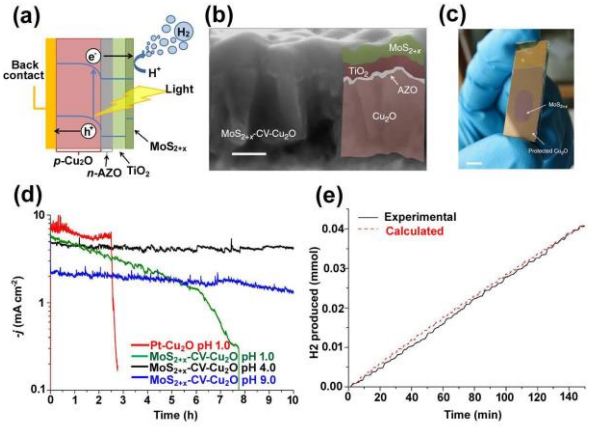

Figure 5. MoS_{2+x}-Cu_2O photocathode, adapted from Ref. [118], reprinted by permission from Macmillan Publishers Ltd, Nature Communications, copyright (2014): (a) Schematic structure of the surface-protected photocathode showing photon absorption and generation of an electron-hole pair in

the p-Cu_2O. The extraction of the excited electron through the TiO_2-protective layer to produce hydrogen on the MoS_{2+x} catalyst is also illustrated. (b) Cross-sectional SEM image of protective layers (20 nm AZO and 100 nm TiO_2) on Cu_2O and a ca. 100 nm of MoS_{2+x} film (CV: by cyclic voltammograms) on top of the protected Cu_2O electrode. Scale bar is 200 nm. (c) A digital image of a MoS_{2+x}-CA-Cu_2O photocathode (CA: by constant anodic photoelectrodeposition). Scale bar is 5 mm. The area covered with the MoS_{2+x} catalyst (66 mg cm^{-2}) is in the middle of the photoelectrode and corresponds here to 0.48 cm^2. (d) Long-term stability and Faradaic efficiency of Photocathode stability at 0 V (vs. RHE) for Cu_2O photocathodes modified by different HER catalysts under constant AM 1.5 illumination. (e) Calculated versus real hydrogen production using a MoS_{2+x}-CA-Cu_2O photocathode (at 0 V) under chopped AM 1.5 irradiation at pH 4.0. The theoretical and experimental values represent the expected and observed amount of H_2 produced, assuming a quantitative Faradaic yield for H_2 formation after an activation process of 20 min.

The pH and applied bias showed a combination of influence on the overall photocathode performance (in Table 1.). Similarly, many compounds showed specific region stability in Pourbaix diagram, both the semiconductor and the electrocatalyst will obey similar rules (either the PEC efficiency or the stability), especially a non-conformal electrocatalyst layer is interfaced with the semiconductor. For instance, the acidic aqueous electrolytes are employed for the photocathodic water splitting. In Figure 6, the silicon based photocathode showed good PEC performance in the acidic or weak acidic solution, by the use of Pt, molybdenum (or tungsten) sulfides, or Mo-Ni HER catalyst. While for Cu_2O materials, weak acidic solutions were widely studied with the protection by TiO_2. The $CuGaSe_2$ | Pt and $CuInS_2$ | In_2S_3 | Pt showed higher photovoltages of 1.1 V and 0.78 V in weak alkaline solution (pH=9~9.5), respectively. However, these materials have not yet showed universal pH range with high efficiency, which potentially requires a tandem cell with ion conductive membrane thus increase the cost. This may partially be due to the higher PEC efficiency since proton concentration is higher in these acidic solutions, or due to the better stability of the photocathodes. Unfortunately, there are not many works showing a clear explanation for this.

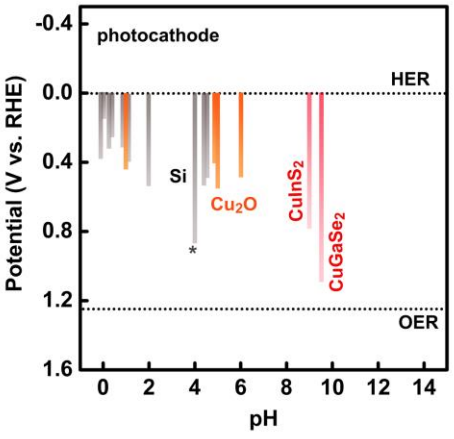

Figure 6. Common earth abundant p-type photocathodes for water reduction in the suitable pH under different external bias. The bottom end of each column corresponded to the positive onset potential V_{on}. The highest active Si shown at pH=4, is made of amorphous Si with p-i-n junction (marked with "*")

Table 1. The PEC performance and stability of photocathode made of earth abundant materials.

Photocathode	Electrolyte	Performance[a, b]	Stability	Ref.
n^+p-Si MWs | Pt	0.5 M K_2SO_4-H_2SO_4 (pH=2)	J_{SC}=15 mA/cm^2, V_{oc}=0.54 V, η=5.8 %	stable for 22 h PEC measurement	[102]
p-SiNWs | Pt (ALD)	0.5 M H_2SO_4	J_{SC}=20.7 mA/cm^2, V_{on}=0.25 V, η≈1.3%	no degradation for 1 h with TiO_2 protection	[103]

p-SiNWs | Pt (ALD)	0.5 M Na_2SO_4-H_2SO_4 (pH=1)	J_{SC} =9 mA/cm^2, V_{on}=0.31 V, η= 1.53%	negligible degradation	[104]
p-Si pillars | Mo_3S_4	1 M $HClO_4$	J_{SC} =9.28 mA/cm^2, V_{on}=0.15 V, η=1.21%	5% decay in first 30 min, then stable 24 h	[111]
SiNWs | $Ni_{12}P_5$	0.05 M H_2SO_4- 0.5 M K_2SO_4	J_{SC}=21 mA/cm^2, V_{oc}=0.4 V, η=2.97%	3% decay in 600 s, then stable	[112]
n^+p-Si planar | Ni-Mo	0.2 M KHP-0.5 M K_2SO_4-KOH (pH=4.5)	J_{SC}=22.3 mA/cm^2, V_{oc}= 0.526 V, η=3.6%	-	[113]
n^+p-Si MWs | Ni-Mo	0.2 M KHP-0.5 M K_2SO_4-KOH (pH=4.5)	J_{SC} =10.3 mA/cm^2, V_{oc} =0.49 V, η=2.2%	9% decay for 4000 s	[113]
a-Si | TiO_2 | Ni-Mo	0.5 M potassium hydrogen phthalate (KHP) (pH=4)	J_{SC} =11.12 mA/cm^2, V_{on}=0.87 V, η=5.5%	<5% decay in 12 h PEC measurements	[114]
p-SiNWs | a-WS_3	0.05 M H_2SO_4 - 0.5 M K_2SO_4	J_{SC} =19.0 mA/cm^2, V_{oc}= 0.4 V, η=2.02%	stable over 20 min	[115]
n^+p Si | Ti | MoS_x	1 M $HClO_4$	J_{SC} =16.3 mA/cm^2, V_{oc}=0.38 V, η=7.56%	~7% decay of J_{SC} for 1 h	[116]
n^+p Si | MoS_2	0.5 M H_2SO_4	J_{SC}=17 mA/cm^2, V_{oc}=0.32 V, η=1.6%	no decrease for 100 h measurement	[120]
p-Cu_2O | AZO, TiO_2 | Pt	1 M Na_2SO_4- 0.1 M KPi (pH=4.9)	J_{SC}=5.7 mA/cm^2, V_{on}=0.4 V, η≈0.57%	active in 1 h, 22% decay in 20 min	[106]
Cu_2O | NiO_x	1 M Na_2SO_4 (pH=6)	J_{SC}≈5.2 mA/cm^2,[c] V_{on}≈0.48 V, η≈ 2.2%	43% decay after 20 min	[117]
Cu_2O | AZO | TiO_2 | MoS_{2+x}	0.1 M H_2SO_4 (pH=1)	J_{SC}=5.7 mA/cm^2, V_{on}=0.45 V, η≈0.85%	50% decay for 5 h	[118]
Cu_2O | AZO,TiO_2 | RuO_2	0.1 M phosphate -0.5 M Na_2SO_4 (pH = 5.0)	J_{SC}=5 mA/cm^2, V_{on}=0.55 V, η=6%	94% stability for 8 h	[119]
$CuGaSe_2$ | Pt	0.1 M Na_2SO_4-NaOH (pH=9.5)	J_{SC}=4.8 mA/cm^2, V_{on}= 1.1 V, η=0.35 %	-	[108]
$CuInS_2$ | In_2S_3 | Pt	0.1 M Na_2SO_4 (pH=9)	J_{SC}=15 mA/cm^2, V_{on}=0.78 V, η=2%	63% decay after 3 h at 0 V	[109]

Note:

a. Power converting efficiency η in three electrode configuration is used here.

b. V_{on} and V_{oc} correspond to the onset potential and open-circuit potential (all the V_{on} is referenced to the RHE, unless specified), which may have a small difference depending on the overpotential of each electrocatalyst for HER. J_{SC} is the current at the potential at 0 V vs. RHE.

c. Solar light power density is 26 mW/cm^2

4. Oxygen evolution reaction

Compared with the hydrogen evolution reactions on photocathode, the oxygen evolution reactions (OER) on photoanode is more challenging. This is due to the oxygen evolution reactions require 4 holes reacting with water molecules (or hydroxyl anions) to form one O_2 molecule, an inherently sluggish process. Seitz et al. showed that the overpotentials for OER on RuO_2 or MnO_x electrocatalyst is much larger than that for HER on Pt or MoS_2 electrocatalyst to achieve same current density [21]. Thus, the development of stable, high-performance photoanode is critically needed.

Transition metal oxides catalysts such as IrO_x and RuO_x are the state-of-art OER electrocatalysts, with onset potentials as low as of 1.44 V and 1.34 V, and Tafel slope of 40 mV/dec, respectively [121]. Although these precious transition metal oxides catalyst are scarce and expensive for practical large scale water splitting applications, the study on the applying these electrocatalysts on semiconductors can be used to demonstrate the validation of the semiconductor-electrocatalyst strategy. Further studies on the earth abundant OER catalysts [41], for instance, Co-Pi [122], Co, $Co(OH)_x$, Co_3O_4, $NiFeO_x$ [123], $CoFeO_x$, FeOOH, NiOOH, $NiRuO_x$, Ni, NiO, MnO and MnO_x may contribute significantly to the development of practical photoanodes.

4.1 IrO_x or RuO_x assisted OER

As mentioned above, the state-of-art OER catalysts, e.g. IrO_x and RuO_x, have been successfully incorporated onto the n-type semiconductors for improved PEC efficiency and stability. For example, in 2010, Tilley et al. [51] prepared cauliflower-like Fe_2O_3 films on FTO by APCVD. On this unique nanostructure, the IrO_2 OER catalyst was used to enhance the charge transfer kinetics, where a high photocurrent of 3.14 mA/cm^2 at 1.23 V and a V_{on} of 0.81 V was achieved in 1 M NaOH, corresponding to a power conversion efficiency of 0.32%. The photocurrent showed a 9% decay for 200 s, which might be due to the de-atachement of the catalyst from hematite. Additionally, RuO_2 has been applied onto nickel doped indium-tantalum-oxide, $In_{1-x}Ni_xTaO_4$ (x = 0-0.2) [124], and $NiRuO_x$ was applied onto nanostructured Si [125], for the same purposes of enhancing OER activities.

4.2 Cobalt-based catalyst assisted OER

As one kind of earth abundant materials, cobalt based OER catalysts, including simple Co or CoO_x, has received the most attention. For instance, TiO_2 photoanode incorporated with Co catalyst showed a photocurrent of ca. 0.39 mA/cm^2, and a power conversion efficiency of ~0.16% [126]. A further improved performance was observed on a nitrogen-doped TiO_2 photoelectrode. A similar conclusion was achieved on mesoporous Fe_2O_3|CoO films by Diab et al. [127], $BiVO_4$| CoO_x (1 nm) by Lichterman et al. [128], and Ta_3N_5| Co_3O_4 nanoparticles by Liu et al. [129]. Additionally, Reece et al. deposited cobalt borate catalyst (Co-OEC) on a triple junction of amorphous Si photovoltaic devices and coupled with NiMoZn HER catalysts in a wired PEC cell or wireless cell [35]. A power conversion efficiency of 4.7% was obtained in 1 M K-borate solution.

Cobalt phosphate (Co-Pi**)** is another earth abundant OER catalyst [122], which can be incorporated onto various n-type semiconductors to enhance PEC water oxidation performance. In 2013, Kim et al. [130] prepared Co-Pi catalyst onto a single crystalline "worm-like" Pt-doped Fe_2O_3 nanostructured films, which led to a high power conversion efficiency of 0.6%. Recently, Qiu and his coworkers deposited ultrathin hematite films onto a three-dimensional (3D) nanophotonic structure [131]. The 3D hematite films incorporated with Co-Pi catalyst resulted in a photocurrent up to 3.05 mA/cm^2 at 1.23 V (vs. RHE) in 1 M NaOH and a low V_{on} at 0.75 V, corresponding to the power efficiency of 0.45%. Li et al. [132] reported an efficient and stable

photoanode combining the barium-doped Ta_3N_5 nanostructures and stable cobalt phosphate electrocatalyst. Abdi et al. prepared 1% W-doped $BiVO_4$ by spray pyrolysis [133]. By using Co-Pi (electrodeposition, 30 nm) as an OER catalyst, they measured a photocurrent of 2.3 mA/cm^2 and a V_{on} of 0.66 V in 0.5 M K_2SO_4 solution (pH=5.6) or 0.1 M potassium phosphate. Abdi and his coworkers have also prepared a gradient dopant of tungsten in a $BiVO_4$ film, forming a distribution of n^+-n homojunction, where the conversion efficiency was further improved [79].

4.3 Nickel-based catalyst assisted OER

Nickel based oxides or hydroxides, as another kind of earth abundant OER catalysts, have also shown dramatic catalytic improvement on the photoanode. Very recently, Kenney et al., has deposited a Ni film (varying between 2-20 nm) on n-Si by electron beam evaporation, which formed a n-Si | Ni/NiO structures as photoanode [10]. The photoanode was protected by the Ni/NiO layer, where the overpotential increased about 0.09 V for 1 h PEC test.

As mentioned above, with the protection of n-Si by TiO_2 conformal layer, the stability of the Si photoanode could be significantly increased. Hu and coworkers deposited TiO_2 on n-Si by ALD to prevent corrosion, followed by Ni thin films or islands on (in Figure 7) [11]. The photogenerated holes transport through the TiO_2 interlayer to Ni/Ni oxide islands/films to oxidize water to O_2, instead of promoting the photocorrosion of the underlying anode. The buried junction, formed by TiO_2 overlayer, produced a characteristic photovoltage of 0.5~0.55 V under illumination. The n-Si | TiO_2 | Ni photoanode exhibited 12.4 mA/cm^2 and V_{on} potential at 1.06 V (with 1.25 sun illumination) in 1 M KOH. Additionally, the photoanode showed impressive stability with continuous oxidation of water to O_2 after more than 100 hours of photocurrent higher than 30 mA/cm^2. Similar protection and catalytic results were obtained on a n-p^+ GaAs | TiO_2 | Ni photoanode, where the power conversion efficiency reached to 3.6% and there was only 8% photocurrent decay after 25 hours.

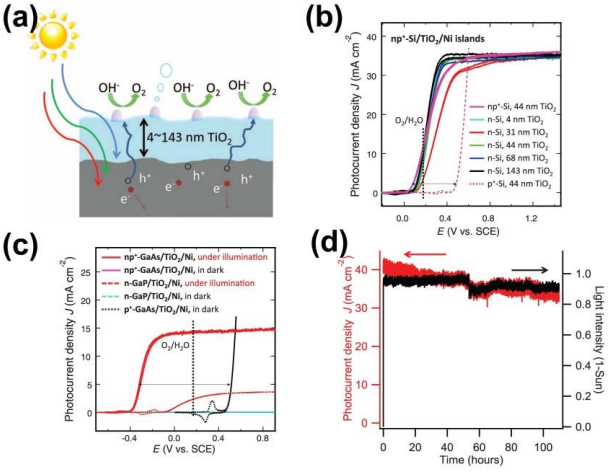

Figure 7. Photodriven water oxidation on protected semiconductors in 1.0 M KOH (aq.), adapted from Ref. [11] reprinted with permission from AAAS: (a) Cross-sectional schematic of a photoanode stabilized against corrosion by a thick electronically defective layer of unannealed TiO_2 deposited by ALD. Instead of corroding the anode, the photogenerated holes are conducted through the TiO_2 to Ni electrocatalysts, where the holes are used to oxidize water to O_2. (b) Photoelectrochemical behavior of the Si photoelectrodes (n-Si, np^+-Si) were tested under ELH-type W-halogen simulated solar illumination at 1.25 Sun, and the 100-nmthick Ni-island electrocatalysts were patterned in square arrays of 3-mmdiameter circles on a 7-mm pitch. (c) The 2 nm Ni/118 nm TiO_2-coated np^+-GaAs and n-GaP photoelectrodes were tested under simulated AM 1.5 illumination at 1 Sun and in the dark. (d) Chronoamperometry of an n-p^+-Si photoanode coated with 44 nm of TiO_2 and Ni islands for over 100 hours illumination (1.25 Sun) at 0.93 V versus SCE in 1.0 M KOH (aq). The photocurrent density versus time (red curve) was overlaid with the illumination intensity versus time (black curve).

Kim and Choi had applied two different OER catalysts, FeOOH and NiOOH onto $BiVO_4$ serially as an efficient photoanode [134]. The photocurrent was as high as 4.1 mA/cm^2 and the V_{on} was as low as 0.2 V in 0.5 M potassium phosphate (pH=7), resulting in power conversion efficiency to 1.75%. More importantly, there was no obvious photocurrent decay after

measurement for 48 h.

4.4 Mn-based catalyst assisted OER

Like many other earth abundant metal oxide OER catalysts, manganese-based electrocatalysts are regarded as promising materials that can interface with the n-type semiconductors. Liu et al. has prepared crystalline WO_3 thin films on planar FTO and $TiSi_2$ nanonets substrates by ALD [52]. With a novel Mn-based OER catalyst coated on, the WO_3 photoanode showed the photocurrent was about 2.1 mA/cm^2 and a V_{on} at 0.39 V in 1 M KCl-HCl (pH=2~7) electrolyte, corresponding to a power conversion efficiency of ca. 0.62%. More interestingly, the photocurrent on WO_3 decayed only 4% after 1 h, and a 50% decay when soaking in H_2O (pH=7) under illumination. Strandwitz et al. have deposited 10 nm MnO films on n-Si as a photoanode by ALD, which showed a photocurrent at about 5.1 mA/cm^2 and a V_{on} potential at 1.11 V [135]. The obtained photoanode showed stable PEC performance for 10-30 minutes.

4.5 Iron based catalyst assisted OER

Iron based OER electrocatalysts have also attracted increasing research attention, due to its high OER catalytic performance and earth abundance. Du and her coworkers prepared hematite thin films (25 nm) by ALD, which was decorated by an amorphous $NiFeO_x$ OER catalyst film [136]. The onset potential was dramatically shifted to 0.58 V in 1 M NaOH. There was no measurable photocurrent decay for 5 h PEC testing. Seabold et al. reported by using a photodeposition method, a FeOOH layer (~110 mg/cm^2, calculated via 100% faradaic efficiency) as OER catalyst was coupled on $BiVO_4$ as a photoanode [24]. In 0.1 M potassium phosphate solution (pH=7), the photocurrent of 2.3 mA/cm^2 and a low V_{on} of 0.25 V were measured, showing a power conversion efficiency was about 0.79%. Chemelewski et al. has reported an amorphous FeOOH by electrodeposition on amorphous Si (triple junctions) as a photoanode, which showed the photocurrent at 4.3 mA/cm^2 in 0.5 M $NaHCO_3$-0.5 M Na_2CO_3 solution and a 4.3% power conversion [137].

Klepser et al. has prepared Fe(tebppmcm)Cl as an OER molecular catalyst on WO_3 films by use of the phosphonate anchors, which significantly increase the stability of the photoanode up to 3 h oxygen evolution test comparing the common carboxylate anchors on hematite [138]. In 0.1 M Na_2SO_4 (pH=3) electrolyte, the photocurrent of 0.99 mA/cm^2 and V_{on} potential of 0.7 V were achieved, corresponding to the power conversion efficiency of 0.17%.

Based on the results summarized above, it is clear that many earth abundant OER catalysts have been successfully used to enhance the PEC water oxidation on various n-type semiconductors. More details of recent literature results in this area are listed in Table 2.

Table 2. The PEC performance and stability of photoanode made of earth abundant materials.

Photoanode	Electrolyte	Performance[a,b]	Stability	Ref.
α-Fe_2O_3 | IrO_2	1 M NaOH (pH=13.6)	J_{SC}≈ 3.14 mA/cm^2, V_{on} ≈ 0.81 V, η ≈0.32%	9% decay in 200 s	[51]
n-Si | $NiRuO_x$	0.25 M Na_2SO_4 (pH=7.2)	J_{SC} =1.5 mA/cm^2, V_{on} =0.93 V, η =0.13%	50% decay in 1 h	[125]
N-doped TiO_2 | Co	1 M KOH (pH=13.5)	J_{SC}=0.62 mA/cm^2, V_{on}=0.47 V, η≈0.23%	no significant change for 10 min	[126]

Fe_2O_3 | CoO	1 M KOH	J_{SC} ≈0.70 mA/cm^2, V_{on} ≈ 0.64 V, η ≈ 0.08%	1% decay for 7.5 min	[127]
$BiVO_4$ | CoO_x	KOH (pH=13)	J_{SC} ≈1.58 mA/cm^2, V_{on} ≈ 0.42 V, η ≈ 0.43%	7% decay for 10 min	[128]
a-Si | Co-OEC (3jn-a-Si)	1 M K-Borate (pH=9.2)	J_{SC} =3.5 mA/cm^2 (0 V), V_{on} = -0.4 V, η ≈4.7%[c]	stable for 3 h,	[35]
Ta_3N_5 | FH | Co_3O_4	1 M NaOH (pH=13.6)	J_{SC} ≈ 5.2 mA/cm^2, V_{on} ≈ 0.60 V, η ≈ 0.72%	6% decay after 6 h	[129]
Pt doped α-Fe_2O_3 | Co-Pi	1 M NaOH	J_{SC}=4.32 mA/cm^2, V_{on} ≈ 0.65 V, η =0.6%	slight decay in 3 h.	[130]
Fe_2O_3 (3D) | Co-Pi	1 M NaOH (pH=13.6)	J_{SC} ≈ 3.05 mA/cm^2, V_{on} ≈ 0.75 V, η ≈ 0.45%	-	[131]
Ba-Ta_3N_5 | Co-Pi	0.5 M K_2HPO_4 (pH=13)	J_{SC} ≈ 6.7 mA/cm^2, V_{on} ≈ 0.65 V, η ≈1.5%	5% decay for 100 min	[132]
W:$BiVO_4$ | Co-Pi	0.5 M K_2SO_4 (pH≈5.6)	J_{SC} = 2.3 mA/cm^2, V_{on} ≈ 0.66 V, η ≈ 0.27%	-	[133]
W:$BiVO_4$ | Co-Pi	0.1 M KPi (pH≈7.3)	J_{SC} = 3.6 mA/cm^2, V_{on} ≈ 0.31 V, η ≈ 1.3%	no obvious decay in 1 h	[79]
Fe_2O_3 | $NiFeO_x$	1 M NaOH (pH=13.6)	J_{SC} ≈ 0.56 mA/cm^2, V_{on} ≈ 0.58 V, η ≈ 0.09%	no measurable decay for 5 h.	[136]
n-Si | Ni/NiO (2nm Ni)	1 M KOH (pH=14)	J_{SC} =14 mA/cm^2,[d] V_{on} =1.05 V, η =0.25%	overpotential increase 0.09 V for 1h PEC	[10]
Si | TiO_2 | Ni	1 M KOH	J_{SC} =12.4 mA/cm^2,[e] V_{on} =1.06 V, η =0.28%	10% decay for 100h	[11]
WO_3 | Mn catalyst	1 M KCl-HCl (pH=2~7)	J_{SC} ≈ 2.1 mA/cm^2, V_{on} ≈ 0.39 V, η ≈0.62%	4% decay in 1 h, 50% decay for 19 h	[52]
n-Si | MnO	1 M KOH (pH=13.6)	J_{SC} =5.1 mA/cm^2, V_{on} =1.11 V, η =0.27%	stable 10-30 min	[135]
WO_3 | Fe(tebppmcn)Cl_2	0.1 M Na_2SO_4 (pH=3)	J_{SC} ≈ 0.99 mA/cm^2, V_{on} ≈ 0.7 V, η ≈0.17%	no obvious decay for 3 h test.	[138]
$BiVO_4$ | FeOOH	0.1 M KPi (pH=7)	J_{SC} ≈2.3 mA/cm^2, V_{on} ≈ 0.25 V, η ≈ 0.79%	2% decay for 6 h	[24]
$BiVO_4$ | FeOOH/ NiOOH	0.5 M KH_2PO_4 (pH=7)	J_{SC} =4.1 mA/cm^2, V_{on} =0.2 V, η =1.75%	no decay for 48 h	[134]
a-Si | a-FeOOH (3jn)	0.5 M $NaHCO_3$-0.5 M Na_2CO_3	J_{SC} =4.3 mA/cm^2, η =4.3%	no degradation for 4 h	[137]

Note:

a. the power conversion efficiency is read and calculated based on the *J-V* curves from the literatures, which is mostly running in a three electrodes configuration.

b. V_{on} is read from the *J-V* curves (reference to RHE), where the anodic current increase. J_{SC} is the current at the potential at 1.23 V vs. RHE.

c. The STH efficiency in two electrode configuration was used here.

d. Photocurrent was measured under 2 sun (corresponding to 200 mW/cm^2).

e. Photocurrent was measured under 1.25 sun (corresponding to 125 mW/cm^2).

However, semiconductor based photoanodes typically only generate moderate photovoltage (V_{ph} < 1.23 V, usually 0.4-0.6 V). It is far from enough to power complete PEC water splitting reactions without additional energy supplies, either from an external bias or additional photovoltages from photocathodes in a tandem cell configuration or a side-by-side configuration. There, however, exists a critical challenge in this approach because most photoanodes are only stable in alkaline solutions (in Figure 8), whereas photocathodes work the best in acidic solutions. From an engineering perspective, it is important to develop photoelectrodes that are compatible with each other for the construction of complete water splitting systems.

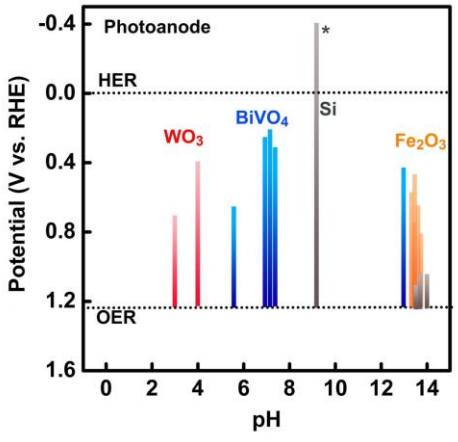

Figure 8. Common earth abundant n-type photoanodes for water oxidation in the suitable pH under different external bias. The top end of each column corresponded to the negative onset potential V_{on}. The Si showed very impressive performance at pH=9.2 is made of 3 junctions amorphous materials, marked with "*".

5. Interface Engineering

While the application of electrocatalysts is expected to improve water splitting kinetics, their introduction may also create new interfaces that will further complicate the operation of photoelectrode performance. For example, it has been shown that some of the PEC characteristics have changed dramatically with the incorporation of electrocatalysts [33]. Ideally, the electrocatalysts should simply function to provide an alternative reaction pathway to accelerate photogenerated charge transfer to lower the kinetic overpotentials. One of the critical factors that ensure the realization of this goal is the presence of ohmic contact between the catalyst and the buried semiconductors. Such an assumption is rarely met in realistic cases. As such, we envision the following are important issues to consider when constructing practical photoelectrode systems that involve catalysts.

1) An interlayer that enables fast charge transfer from the photoabsorber to catalyst overlayer with no or low junction barrier is critical. The interlayer between the light absorber and catalyst forms ohmic contact with each layer. The interlayer may allow us to optimize both sides independently and also make the material integration successful. For example, by using crystalline Si with buried junctions (n-p$^+$ Si) as a photoabsorber, Cox et al. [139] studied different interlayers (ITO, FTO and Ni) in combination with various OER catalysts (CoBi, NiBi, and NiFeO). Tafel behaviors were studied under dark and illumination, confirming that the main factors of influence were catalysis and interface resistance of the cells. Moreover, a suitable

alignment of TiO_2 conduction band is achieved relative to the HER potential on n^+p Si photoanode, allowing the electrons flow from Si to Pt freely [95].

2) The electronic structures at the interface need to be studied with great care. Electronic states with energies in the band gap of the semiconductor can serve as recombination centers to pin the Fermi level, which in turn will limit measurable photovoltages [140]. The new formed interface between semiconductor and electrocatalyst could also generate large amount of defects, causing charge recombination and significantly influence the band structures near interface (in Figure 9). Recently work by Yang et al. has shown that hematite coated with MnO_x OER catalyst by ALD method exhibited significant anodic onset potential shift (in Figure 10a) [141]. The results confirmed that the photovoltage generated by hematite had been severely diminished (in Figure 9c). In stark contrast, similar MnO OER catalyst improved PEC performance of n-Si [135]. Along the same line, Sivula and coworkers showed that the V_{on} and PEC performance of hematite could be readily improved by coating Al_2O_3, Ga_2O_3 and In_2O_3 non-catalytic overlayers using ALD [29, 30]. More recently, it was confirmed that a TiO_2 non-electrocatalyst deposited on hematite by ALD also reduced surface states, leading to measureable PEC performance improvement. The surface charge recombination was found to be suppressed and the photovoltage increased resulting in a cathodic shift of V_{on} was observed (in Figure 10b) [31].

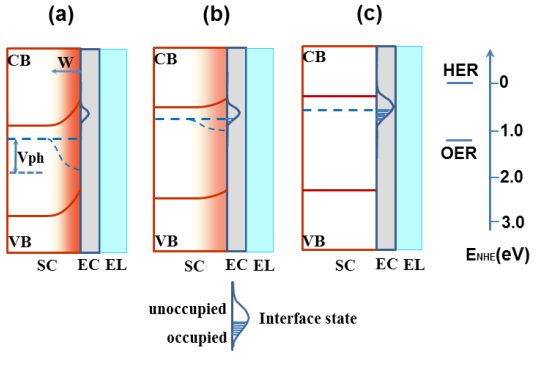

Figure 9. Schematic structures of n-type semiconductor (SC) photoanode interfaced with electrocatalyst (EC) layer showing the charge recombination at the various interface states equilibrium with the electrolyte (EL): a) Moderate band bending with little surface states, (b) partial Fermi-Level pinning due to the emptying the interface state, showed less band bending, (c) serious Fermi-Level pinning due to the huge interface state, showed no band bending.

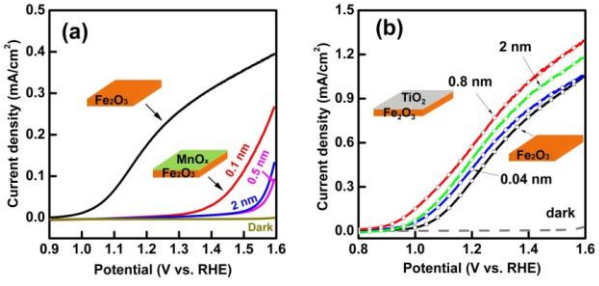

Figure 10. *J-V* plots of hematite with and without modification layer by ALD in 1.0 M NaOH aqueous electrolyte under simulated solar illumination (AM 1.5, 100 mW/cm^2). (a) MnO_x OER electrocatalyst decoration layer, adapted from Journal of Catalysis, X. Yang et al., ref. [141], copyright (2013) with permission from Elsevier. (b) TiO_2 non-catalyst decoration layer, adapted with permission from Ref.[31], copyright (2014) American Chemical Society. For comparison, the polarization curve of bare hematite without illumination is included (labeled as dark).

3) The nature of the electrocatalysts plays an important role in defining the performance of the integrated photoelectrode systems. To study this point, Lin and Boettcher recently examined the band structures of the TiO_2 | electrocatalyst with different interface configurations. They coated single crystal TiO_2 electrodes with model IrO_x or $Ni(OH)_2$ electrocatalyst [33]. As shown in Figure 11, they found that the redox-active ion-permeable electrocatalysts of $Ni(OH)_2$ or NiOOH generated an "adaptive" semiconductor/electrocatalyst (SC | EC) junctions. The effective Schottky barrier height changed with the oxidation level of electrocatalysts through Fermi level pinning in Figure 11d, due to the storing photogenerated holes. Oxidation of the $Ni(OH)_2$ electrocatalyst by photogenerated holes could lower the Fermi level of $Ni(OH)_2$ to

yield a large effective barrier height and achieve a larger V_{ph} (Figure 11e). This larger V_{ph} further drives electrocatalyst oxidation until the electrocatalyst potential is sufficiently enough for water oxidation reaction. In contrast, a dense, ion-impermeable IrO_x electrocatalysts layer on TiO_2 formed constant-barrier-height "buried" junctions. The positive feedback was absent for TiO_2 | IrO_x because the *burrier height* is fixed in this case.

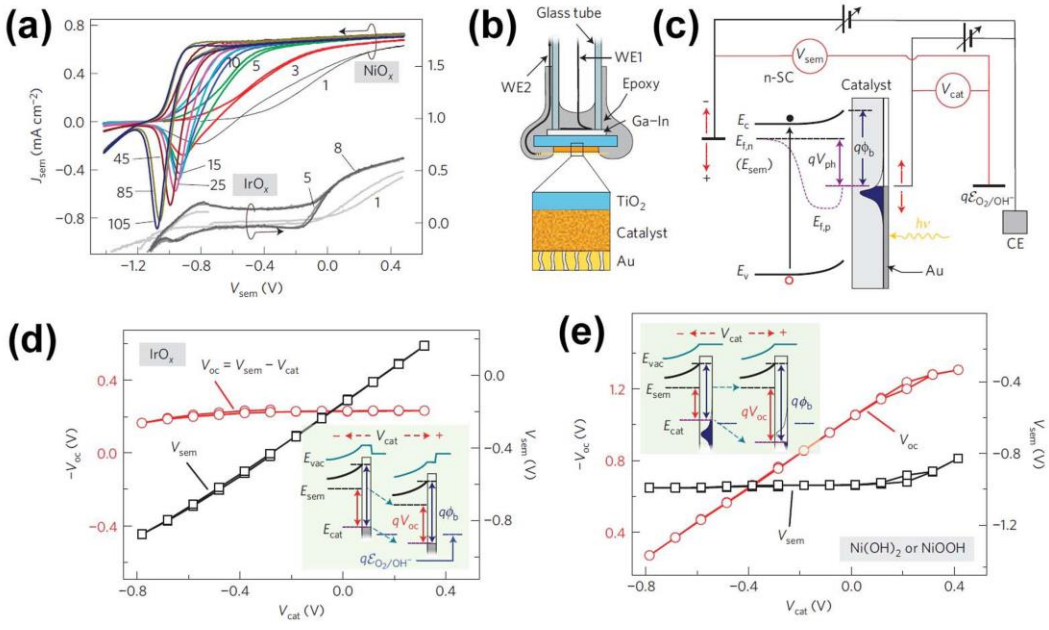

Figure 11. Conventional single-working-electrode *J*–*V* data for TiO_2 | EC samples and schematics of the DWE experiment, adapted from Ref. [33] by permission from Macmillan Publishers Ltd, Nature Materials, Copyright 2014: (a) Evolution of illuminated *J*–*V* curves on repetitive cycling of TiO_2 | NiO_x and TiO_2 | IrO_x electrodes at a scan rate of 100 mV/s and 50 mV/s, respectively, in aqueous 0.1 M KOH under 100 mW/cm^2 of AM1.5G illumination. The cycle number is indicated for each curve. The semiconductor potential V_{sem} is referenced to the thermodynamic redox potential for the OER, $E(O_2/OH^-)$. (b) Device schematic showing independent electrical connections to the SC and EC. (c) Band-bending diagram and wiring schematic for DWE PEC analysis. The TiO_2 potential V_{sem} and the EC potential V_{cat} are controlled relative to $E(O_2/OH^-)$by the primary working electrode (WE1) and the secondary working electrode (WE2), respectively, of a bi-potentiostat (using a single Hg/HgO reference electrode). E_C and E_V are the conduction and valence bands of the SC, respectively. $E_{f,n}$ and $E_{f,p}$ are the quasi Fermi levels for electrons and holes, respectively.

Besides the issues outlined above, the electrocatalyst incorporated on the semiconductor surface will also raise questions on the light absorption. Trotochaud et al. have proposed a model that describes the influence of the colored electrocatalyst on the PEC water splitting performance by an in situ spectroelectrochemistry [142]. For example, CoO_x, $NiCoO_x$, $Ni_{0.9}Fe_{0.1}O$ and IrO_x are generally colored and have competitive light absorption with the semiconducting photoabsorber. Like the very recent work on NiO (Eg=3.7 eV) by Mei et al. [143], the transparent, thickness of a continuous (or discontinuous) electrocatalyst film should be optimized when interfaced with the semiconductors.

6. Summary and outlook

The rapid development on PEC water splitting in the past decades provides an opportunity to gain a profound understanding of the field. Scientists have not only designed new light absorber materials, such as heteronanostructures, but have also engineered interfaces of various components to improve the power conversion efficiencies and photoelectrode stabilities. Various earth abundant electrocatalyst-assisted PEC water splitting systems have shown promising performances, either by the improved charge separation, transfer or by surface protection. In some cases, although the photovoltage can be enhanced by the interface layer and electrocatalysts, the modest increases are insufficient to complete water splitting. Many photoelectrodes were measured in three-electrode configuration with an external applied bias. As a result, the reported efficiencies of photoelectrodes are often less than reliable. Of the relatively high-efficiency demonstrations, materials require complex fabrication to generate high V_{ph}, such as Si triple junctions or Si-based solar cells, are often used. Recently, two examples with higher STH efficiencies systems were reported based on the perovskite tandem photovoltaics [144] or Si minimodules [145], combined with earth abundant electrocatalysts. Their presence increases the overall fabrication cost.

Within this context, we view the requirements for further development of earth-abundant materials for PEC waters splitting is urgent. The demands include the development of new, earth abundant semiconductors, with suitable band gap and band edge positions. They also include the development of transparent, high-performance electrocatalysts for both OER and HER. Great attention needs to be focused on the interfaces between the semiconductors and the catalysts. Stability is another important concern which needs to be address. The resulting photoelectrodes should be stable for years, not just several hours. They need to survive under harsh conditions such as operation environmental temperatures, unstable illumination, wide variations of pH, periodical current flows, and varying ionic strengths. Engineering of a practical water splitting device will require significant attention as well. How to separate the two products (H_2 and O_2) remains a pressing challenge. If not properly managed, product cross-over not only reduces the overall efficiencies, but also poses serious safety hazards. Because PEC devices are ultimately limited by light intensities, they tend to operate at significantly lower current densities than existing commercial electrolyzers. As such, new membranes that are less permeable to O_2 and H_2 are needed. As daunting as the challenges may seem, the hopes are high. Significant research efforts have been attracted to this important problem. The interest is largely driven by the sense of urgency distilled by the potential devastation of our delicate environmental system by continued fossil fuel usage. We are optimistic that low-cost, high-efficiency solar water splitting is not only possible, and it is within our reach in the near future.

Acknowledgements

This work was supported by Boston College, NSF (DMR 1055762 and 1317280), and MassCEC. R.L. is supported by the Joint Center for Artificial

Photosynthesis, a DOE Energy Innovation Hub, supported through the Office of Science of the U.S. Department of Energy under Award Number DE-SC0004993. We thank partial support by Program for Innovative Research Team (in Science and Technology) in University of Henan Province (No.2012IRTSTHN021), Innovation Scientists and Technicians Troop Construction Projects of Henan Province (No. 144200510014) and National Natural Science Foundation of China (No. 21273192). D.W. is an Alfred P. Sloan Fellow.

References

[1] *BP Statistical Review of World Energy* BP Plc, 2014.

[2] Nocera, D. G. The artificial leaf. *Acc. Chem. Res.* **2012**, *45*, 767-776.

[3] Liu, C.; Dasgupta, N. P.; Yang, P. Semiconductor nanowires for artificial photosynthesis. *Chem. Mater.* **2013**, *26*, 415-422.

[4] *Evert*, R. F.; Eichhorn, S. E. *Biology of Plants*; W.H. Freeman and Company Publishers: New York, 2005.

[5] Walter, M. G.; Warren, E. L.; McKone, J. R.; Boettcher, S. W.; Mi, Q. X.; Santori, E. A.; Lewis, N. S. Solar water splitting cells. *Chem. Rev.* **2010**, *110*, 6446-6473.

[6] Boddy, P. J. Oxygen evolution on semiconducting TiO_2. *J. Electrochem. Soc.* **1968**, *115*, 199-203.

[7] Fujishima, A.; Honda, K. Electrochemical photolysis of water at a semiconductor electrode. *Nature* **1972**, *238*, 37-38.

[8] Aharon-Shalom, E.; Heller, A. Efficient p-lnP(Rh-H alloy) and p-lnP(Re-H alloy) hydrogen evolving photocathodes. *J. Electrochem. Soc.* **1982**, *129*, 2865-2866.

[9] Licht, S.; Wang, B.; Mukerji, S.; Soga, T.; Umeno, M.; Tributsch, H. Efficient solar water splitting, exemplified by RuO_2-catalyzed AlGaAs/Si photoelectrolysis. *J. Phys. Chem. B* **2000**, *104*, 8920-8924.

[10] Kenney, M. J.; Gong, M.; Li, Y.; Wu, J. Z.; Feng, J.; Lanza, M.; Dai, H. High-performance silicon photoanodes passivated with ultrathin nickel films for water oxidation. *Science* **2013**, *342*, 836-840.

[11] Hu, S.; Shaner, M. R.; Beardslee, J. A.; Lichterman, M.; Brunschwig, B. S.; Lewis, N. S. Amorphous TiO_2 coatings stabilize Si, GaAs, and GaP photoanodes for efficient water oxidation. *Science* **2014**, *344*, 1005-1009.

[12] van de Krol, R. Principles of Photoelectrochemical Cells. In *Photoelectrochemical Hydrogen Production*. R. van de Krol; M. Grätzel, Eds.; Springer US, 2012; pp 13-67.

[13] Andrade, L.; Lopes, T.; Ribeiro, H. A.; Mendes, A. Transient phenomenological modeling of photoelectrochemical cells for water splitting - Application to undoped hematite electrodes. *Int. J. Hydrogen Energy* **2011**, *36*, 175-188.

[14] Hu, S.; Xiang, C.; Haussener, S.; Berger, A. D.; Lewis, N. S. An analysis of the optimal band gaps of light absorbers in integrated tandem photoelectrochemical water-splitting systems. *Energy Environ. Sci.* **2013**, *6*, 2984-2993.

[15] Haussener, S.; Xiang, C.; Spurgeon, J. M.; Ardo, S.; Lewis, N. S.; Weber, A. Z. Modeling, simulation, and design criteria for photoelectrochemical water-splitting systems. *Energy Environ. Sci.* **2012**, *5*, 9922-9935.

[16] Woodhouse, M.; Parkinson, B. A. Combinatorial approaches for the identification and optimization of oxide semiconductors for efficient solar photoelectrolysis. *Chem. Soc. Rev.* **2009**, *38*, 197-210.

[17] Lide, D. R. *CRC Handbook of Chemistry and Physics*; CRC Press, 2003.

[18] Sathre, R.; Scown, C. D.; Morrow, W. R.; Stevens, J. C.; Sharp, I. D.; Ager, J. W.; Walczak, K.; Houle, F. A.; Greenblatt, J. B. Life-cycle net energy assessment of large-scale hydrogen production via photoelectrochemical water splitting. *Energy Environ. Sci.* **2014**, *7*, 3264-3278.

[19] Pinaud, B. A.; Benck, J. D.; Seitz, L. C.; Forman, A. J.; Chen, Z.; Deutsch, T. G.; James, B. D.; Baum, K.

N.; Baum, G. N.; Ardo, S.; Wang, H.; Miller, E.; Jaramillo, T. F. Technical and economic feasibility of centralized facilities for solar hydrogen production via photocatalysis and photoelectrochemistry. *Energy Environ. Sci.* **2013**, *6*, 1983-2002.

[20] Bolton, J. R.; Strickler, S. J.; Connolly, J. S. Limiting and realizable efficiencies of solar photolysis of water. *Nature* **1985**, *316*, 495-500.

[21] Seitz, L. C.; Chen, Z.; Forman, A. J.; Pinaud, B. A.; Benck, J. D.; Jaramillo, T. F. Modeling practical performance limits of photoelectrochemical water splitting based on the current state of materials research. *ChemSusChem* **2014**, *7*, 1372-1385.

[22] Cho, I. S.; Chen, Z.; Forman, A. J.; Kim, D. R.; Rao, P. M.; Jaramillo, T. F.; Zheng, X. Branched TiO_2 nanorods for photoelectrochemical hydrogen production. *Nano Lett.* **2011**, *11*, 4978-4984.

[23] Varghese, O. K.; Grimes, C. A. Appropriate strategies for determining the photoconversion efficiency of water photoelectrolysis cells: a review with examples using titania nanotube array photoanodes. *Sol. Energy Mater. Sol. Cells* **2008**, *92*, 374-384.

[24] Seabold, J. A.; Choi, K. S. Efficient and stable photo-oxidation of water by a bismuth vanadate photoanode coupled with an iron oxyhydroxide oxygen evolution catalyst. *J. Am. Chem. Soc.* **2012**, *134*, 2186-2192.

[25] Zhong, D. K.; Gamelin, D. R. Photoelectrochemical water oxidation by cobalt catalyst ("Co-Pi")/α-Fe_2O_3 composite photoanodes: oxygen evolution and resolution of a kinetic bottleneck. *J. Am. Chem. Soc.* **2010**, *132*, 4202-4207.

[26] Zhong, D. K.; Choi, S.; Gamelin, D. R. Near-complete suppression of surface recombination in solar photoelectrolysis by "Co-Pi" catalyst-modified W:$BiVO_4$. *J. Am. Chem. Soc.* **2011**, *133*, 18370-18377.

[27] Barroso, M.; Cowan, A. J.; Pendlebury, S. R.; Grätzel, M.; Klug, D. R.; Durrant, J. R. The role of cobalt phosphate in enhancing the photocatalytic activity of α-Fe_2O_3 toward water oxidation. *J. Am. Chem. Soc.* **2011**, *133*, 14868-14871.

[28] Gamelin, D. R. Water splitting: catalyst or spectator? *Nat. Chem.* **2012**, *4*, 965-967.

[29] Le Formal, F.; Tetreault, N.; Cornuz, M.; Moehl, T.; Grätzel, M.; Sivula, K. Passivating surface states on water splitting hematite photoanodes with alumina overlayers. *Chem. Sci.* **2011**, *2*, 737-743.

[30] Hisatomi, T.; Le Formal, F.; Cornuz, M.; Brillet, J.; Tetreault, N.; Sivula, K.; Grätzel, M. Cathodic shift in onset potential of solar oxygen evolution on hematite by 13-group oxide overlayers. *Energy Environ. Sci.* **2011**, *4*, 2512-2515.

[31] Yang, X.; Liu, R.; Du, C.; Dai, P.; Zheng, Z.; Wang, D. Improving hematite-based photoelectrochemical water splitting with ultrathin TiO_2 by atomic layer deposition. *ACS Appl. Mater. & Interfaces* **2014**, *6*, 12005-12011.

[32] Liao, M.; Feng, J.; Luo, W.; Wang, Z.; Zhang, J.; Li, Z.; Yu, T.; Zou, Z. Co_3O_4 nanoparticles as robust water oxidation catalysts towards remarkably enhanced photostability of a Ta_3N_5 photoanode. *Adv. Funct. Mater.* **2012**, *22*, 3066-3074.

[33] Lin, F.; Boettcher, S. W. Adaptive semiconductor/electrocatalyst junctions in water-splitting photoanodes. *Nat. Mater.* **2014**, *13*, 81-86.

[34] Mills, T. J.; Lin, F.; Boettcher, S. W. Theory and simulations of electrocatalyst-coated semiconductor electrodes for solar water splitting. *Phys. Rev. Lett.* **2014**, *112*, 148304.

[35] Reece, S. Y.; Hamel, J. A.; Sung, K.; Jarvi, T. D.; Esswein, A. J.; Pijpers, J. J. H.; Nocera, D. G. Wireless solar water splitting using silicon-based semiconductors and earth-abundant catalysts. *Science* **2011**, *334*, 645-648.

[36] Vesborg, P. C. K.; Jaramillo, T. F. Addressing the terawatt challenge: scalability in the supply of chemical elements for renewable energy. *RSC Adv.* **2012**, *2*, 7933-7947.

[37] Li, Z.; Luo, W.; Zhang, M.; Feng, J.; Zou, Z. Photoelectrochemical cells for solar hydrogen

production: current state of promising photoelectrodes, methods to improve their properties, and outlook. *Energy Environ. Sci.* **2013**, *6*, 347-370.

[38] Faber, M. S.; Jin, S. Earth-abundant inorganic electrocatalysts and their nanostructures for energy conversion applications. *Energy Environ. Sci.* **2014**, *7*, 3519-3542.

[39] Osterloh, F. E. Inorganic nanostructures for photoelectrochemical and photocatalytic water splitting. *Chem. Soc. Rev.* **2013**, *42*, 2294-2320.

[40] Liu, R.; Zheng, Z.; Spurgeon, J.; Yang, X. Enhanced photoelectrochemical water-splitting performance of semiconductors by surface passivation layers. *Energy Environ. Sci.* **2014**, *7*, 2504-2517.

[41] Sun, K.; Shen, S.; Liang, Y.; Burrows, P. E.; Mao, S. S.; Wang, D. Enabling silicon for solar-fuel production. *Chem. Rev.* **2014**, *114*, 8662-8719.

[42] Hoang, S.; Berglund, S. P.; Hahn, N. T.; Bard, A. J.; Mullins, C. B. Enhancing visible light photo-oxidation of water with TiO_2 nanowire arrays via cotreatment with H_2 and NH_3: synergistic effects between Ti^{3+} and N. *J. Am. Chem. Soc.* **2012**, *134*, 3659-3662.

[43] Liu, B.; Chen, H. M.; Liu, C.; Andrews, S. C.; Hahn, C.; Yang, P. Large-scale synthesis of transition-metal-doped TiO_2 nanowires with controllable overpotential. *J. Am. Chem. Soc.* **2013**, *135*, 9995-9998.

[44] Sivula, K.; Le Formal, F.; Grätzel, M. Solar water splitting: progress using hematite (α-Fe_2O_3) photoelectrodes. *ChemSusChem* **2011**, *4*, 432-449.

[45] Bignozzi, C. A.; Caramori, S.; Cristino, V.; Argazzi, R.; Meda, L.; Tacca, A. Nanostructured photoelectrodes based on WO_3: applications to photooxidation of aqueous electrolytes. *Chem. Soc. Rev.* **2013**, *42*, 2228-2246.

[46] Park, Y.; McDonald, K. J.; Choi, K. S. Progress in bismuth vanadate photoanodes for use in solar water oxidation. *Chem. Soc. Rev.* **2013**, *42*, 2321-2337.

[47] Brillet, J.; Grätzel, M.; Sivula, K. Decoupling feature size and functionality in solution-processed, porous hematite electrodes for solar water splitting. *Nano Lett.* **2010**, *10*, 4155-4160.

[48] Kay, A.; Cesar, I.; Graetzel, M. New benchmark for water photooxidation by nanostructured alpha-Fe_2O_3 films. *J. Am. Chem. Soc.* **2006**, *128*, 15714-15721.

[49] Le Formal, F.; Graetzel, M.; Sivula, K. Controlling photoactivity in ultrathin hematite films for solar water-splitting. *Adv. Funct. Mater.* **2010**, *20*, 1099-1107.

[50] Sivula, K.; Zboril, R.; Le Formal, F.; Robert, R.; Weidenkaff, A.; Tucek, J.; Frydrych, J.; Graetzel, M. Photoelectrochemical water splitting with mesoporous hematite prepared by a solution-based colloidal approach. *J. Am. Chem. Soc.* **2010**, *132*, 7436-7444.

[51] Tilley, S. D.; Cornuz, M.; Sivula, K.; Graetzel, M. Light-induced water splitting with hematite: improved nanostructure and iridium oxide catalysis. *Angew. Chem., Int. Ed.* **2010**, *49*, 6405-6408.

[52] Liu, R.; Lin, Y.; Chou, L. Y.; Sheehan, S. W.; He, W.; Zhang, F.; Hou, H. J. M.; Wang, D. Water splitting by tungsten oxide prepared by atomic layer deposition and decorated with an oxygen-evolving catalyst. *Angew. Chem., Int. Ed.* **2011**, *50*, 499-502.

[53] Ming, T.; Suntivich, J.; May, K. J.; Stoerzinger, K. A.; Kim, D. H.; Shao-Horn, Y. Visible light photo-oxidation in Au nanoparticle sensitized $SrTiO_3$:Nb photoanode. *J. Phys. Chem. C* **2013**, *117*, 15532-15539.

[54] Hassan, N. K.; Hashim, M. R.; Allam, N. K. ZnO nano-tetrapod photoanodes for enhanced solar-driven water splitting. *Chem. Phys. Lett.* **2012**, *549*, 62-66.

[55] Zhen, C.; Wang, L.; Liu, G.; Lu, G. Q.; Cheng, H. M. Template-free synthesis of Ta_3N_5 nanorod arrays for efficient photoelectrochemical water splitting. *Chem. Commun.* **2013**, *49*, 3019-3021.

[56] Ling, Y.; Wang, G.; Wheeler, D. A.; Zhang, J. Z.; Li, Y. Sn-doped hematite nanostructures for photoelectrochemical water splitting. *Nano Lett.*

2011, *11*, 2119-2125.

[57] Ye, H.; Park, H. S.; Bard, A. J. Screening of electrocatalysts for photoelectrochemical water oxidation on W-doped $BiVO_4$ photocatalysts by scanning electrochemical microscopy. *J. Phys. Chem. C* **2011**, *115*, 12464-12470.

[58] Park, H. S.; Lee, H. C.; Leonard, K. C.; Liu, G.; Bard, A. J. Unbiased photoelectrochemical water splitting in Z-scheme device using W/Mo-doped $BiVO_4$ and $Zn_xCd_{1-x}Se$. *ChemPhysChem* **2013**, *14*, 2277-2287.

[59] Holland, K.; Dutter, M. R.; Lawrence, D. J.; Reisner, B. A.; DeVore, T. C. Photoelectrochemical performance of W-doped $BiVO_4$ thin films deposited by spray pyrolysis. *J. Photonics Energy* **2014**, *4*, 041598.

[60] Zhou, M.; Bao, J.; Xu, Y.; Zhang, J.; Xie, J.; Guan, M.; Wang, C.; Wen, L.; Lei, Y.; Xie, Y. Photoelectrodes based upon Mo:$BiVO_4$ inverse opals for photoelectrochemical water splitting. *ACS Nano* **2014**, *8*, 7088-7098.

[61] Song, X. C.; Yang, E.; Liu, G.; Zhang, Y.; Liu, Z. S.; Chen, H. F.; Wang, Y. Preparation and photocatalytic activity of Mo-doped WO_3 nanowires. *J. Nanopart. Res.* **2010**, *12*, 2813-2819.

[62] Cai, G. F.; Wang, X. L.; Zhou, D.; Zhang, J. H.; Xiong, Q. Q.; Gu, C. D.; Tu, J. P. Hierarchical structure Ti-doped WO_3 film with improved electrochromism in visible-infrared region. *RSC Adv.* **2013**, *3*, 6896-6905.

[63] Upadhyay, S. B.; Mishra, R. K.; Sahay, P. P. Structural and alcohol response characteristics of Sn-doped WO_3 nanosheets. *Sens. Actuators, B* **2014**, *193*, 19-27.

[64] Guo, C. X.; Dong, Y.; Yang, H. B.; Li, C. M. Graphene quantum dots as a green sensitizer to functionalize ZnO nanowire arrays on F-doped SnO_2 glass for enhanced photoelectrochemical water splitting. *Adv. Energy Mater.* **2013**, *3*, 997-1003.

[65] Lin, Y. G.; Hsu, Y. K.; Chen, Y. C.; Chen, L. C.; Chen, S. Y.; Chen, K. H. Visible-light-driven photocatalytic carbon-doped porous ZnO nanoarchitectures for solar water-splitting. *Nanoscale* **2012**, *4*, 6515-6519.

[66] Mayer, M. A.; Yu, K. M.; Speaks, D. T.; Denlinger, J. D.; Reichertz, L. A.; Beeman, J. W.; Haller, E. E.; Walukiewicz, W. Band gap engineering of oxide photoelectrodes: characterization of $ZnO_{1-x}Se_x$. *J. Phys. Chem. C* **2012**, *116*, 15281-15289.

[67] Yang, X.; Wolcott, A.; Wang, G.; Sobo, A.; Fitzmorris, R. C.; Qian, F.; Zhang, J. Z.; Li, Y. Nitrogen-doped ZnO nanowire arrays for photoelectrochemical water splitting. *Nano Lett.* **2009**, *9*, 2331-2336.

[68] Cesar, I.; Kay, A.; Martinez, J. A. G.; Grätzel, M. Translucent thin film Fe_2O_3 photoanodes for efficient water splitting by sunlight: nanostructure-directing effect of Si-doping. *J. Am. Chem. Soc.* **2006**, *128*, 4582-4583.

[69] Hu, Y. S.; Kleiman-Shwarsctein, A.; Forman, A. J.; Hazen, D.; Park, J. N.; McFarland, E. W. Pt-doped α-Fe_2O_3 thin films active for photoelectrochemical water splitting. *Chem. Mater.* **2008**, *20*, 3803-3805.

[70] Ingler, W. B.; Khan, S. U. M. Photoresponse of spray pyrolytically synthesized copper-doped p-Fe_2O_3 thin film electrodes in water splitting. *Int. J. Hydrogen Energy* **2005**, *30*, 821-827.

[71] Kleiman-Shwarsctein, A.; Hu, Y. S.; Forman, A. J.; Stucky, G. D.; McFarland, E. W. Electrodeposition of α-Fe_2O_3 doped with Mo or Cr as photoanodes for photocatalytic water splitting. *J. Phys. Chem. C* **2008**, *112*, 15900-15907.

[72] Kumar, P.; Sharma, P.; Shrivastav, R.; Doss, S.; Satsangi, V. R. Electrodeposited zirconium-doped α-Fe_2O_3 thin film for photoelectrochemical water splitting. *Int. J. Hydrogen Energy* **2011**, *36*, 2777-2784.

[73] Cho, I. S.; Lee, C. H.; Feng, Y.; Logar, M.; Rao, P. M.; Cai, L.; Kim, D. R.; Sinclair, R.; Zheng, X. Codoping titanium dioxide nanowires with tungsten and carbon for enhanced photoelectrochemical performance. *Nat. Commun.* **2013**, *4*, 1723.

[74] Zhou, J. K.; Zhang, Y. X.; Zhao, X. S.; Ray, A. K.

Photodegradation of benzoic acid over metal-doped TiO_2. *Ind. Eng. Chem. Res.* **2006**, *45*, 3503-3511.

[75] Mayer, M. T.; Du, C.; Wang, D. Hematite/Si nanowire dual-absorber system for photoelectrochemical water splitting at low applied potentials. *J. Am. Chem. Soc.* **2012**, *134*, 12406-12409.

[76] Shaner, M. R.; Fountaine, K. T.; Ardo, S.; Coridan, R. H.; Atwater, H. A.; Lewis, N. S. Photoelectrochemistry of core-shell tandem junction n-p^+-Si/n-WO_3 microwire array photoelectrodes. *Energy Environ. Sci.* **2014**, *7*, 779-790.

[77] Coridan, R. H.; Arpin, K. A.; Brunschwig, B. S.; Braun, P. V.; Lewis, N. S. Photoelectrochemical behavior of hierarchically structured Si/WO_3 core-shell tandem photoanodes. *Nano Lett.* **2014**, *14*, 2310-2317.

[78] Liu, C.; Tang, J.; Chen, H. M.; Liu, B.; Yang, P. A fully integrated nanosystem of semiconductor nanowires for direct solar water splitting. *Nano Lett.* **2013**, *13*, 2989-2992.

[79] Abdi, F. F.; Han, L.; Smets, A. H. M.; Zeman, M.; Dam, B.; van de Krol, R. Efficient solar water splitting by enhanced charge separation in a bismuth vanadate-silicon tandem photoelectrode. *Nat. Commun.* **2013**, *4*, 2195.

[80] Leroy, C. M.; Maegli, A. E.; Sivula, K.; Hisatomi, T.; Xanthopoulos, N.; Otal, E. H.; Yoon, S.; Weidenkaff, A.; Sanjines, R.; Grätzel, M. $LaTiO_2N/In_2O_3$ photoanodes with improved performance for solar water splitting. *Chem. Commun.* **2012**, *48*, 820-822.

[81] Patil, R.; Kelkar, S.; Naphadeab, R.; Ogale, S. Low temperature grown $CuBi_2O_4$ with flower morphology and its composite with CuO nanosheets for photoelectrochemical water splitting. *J. Mater. Chem. A* **2014**, *2*, 3661-3668.

[82] AlOtaibi, B.; Nguyen, H. P.; Zhao, S.; Kibria, M. G.; Fan, S.; Mi, Z. Highly stable photoelectrochemical water splitting and hydrogen generation using a double-band InGaN/GaN core/shell nanowire photoanode. *Nano Lett.* **2013**, *13*, 4356-4361.

[83] Yokoyama, D.; Minegishi, T.; Jimbo, K.; Hisatomi, T.; Ma, G. J.; Katayama, M.; Kubota, J.; Katagiri, H.; Domen, K. H_2 evolution from water on modified Cu_2ZnSnS_4 photoelectrode under solar light. *Appl. Phys. Express* **2010**, *3*.

[84] Sun, Y.; Sun, Z.; Gao, S.; Cheng, H.; Liu, Q.; Lei, F.; Wei, S.; Xie, Y. All-surface-atomic-metal chalcogenide sheets for high-efficiency visible-light photoelectrochemical water splitting. *Adv. Energy Mater.* **2014**, *4*, 10.1002/aenm.201300611.

[85] Liu, J.; Li, X. B.; Wang, D.; Liu, H.; Peng, P.; Liu, L. M. Single-layer group-IVB nitride halides as promising photocatalysts. *J. Mater. Chem. A* **2014**, *2*, 6755-6761.

[86] Li, W.; Walther, C. F. J.; Kuc, A.; Heine, T. Density functional theory and beyond for band-gap screening: performance for transition-metal oxides and dichalcogenides. *J. Chem. Theory Comput.* **2013**, *9*, 2950-2958.

[87] Yourey, J. E.; Bartlett, B. M. Electrochemical deposition and photoelectrochemistry of $CuWO_4$, a promising photoanode for water oxidation. *J. Mater. Chem.* **2011**, *21*, 7651-7660.

[88] Kato, M.; Yasuda, T.; Miyake, K.; Ichimura, M.; Hatayama, T. Epitaxial p-type SiC as a self-driven photocathode for water splitting. *Int. J. Hydrogen Energy* **2014**, *39*, 4845-4849.

[89] Biswas, S. K.; Baeg, J. O. Enhanced photoactivity of visible light responsive W incorporated $FeVO_4$ photoanode for solar water splitting. *Int. J. Hydrogen Energy* **2013**, *38*, 14451-14457.

[90] Zhang, X.; Ai, Z.; Jia, F.; Zhang, L. Generalized one-pot synthesis, characterization, and photocatalytic activity of hierarchical BiOX (X = Cl, Br, I) nanoplate microspheres. *J. Phys. Chem. C* **2008**, *112*, 747-753.

[91] Hahn, N. T.; Hoang, S.; Self, J. L.; Mullins, C. B. Spray pyrolysis deposition and photoelectrochemical properties of n-Type BiOI nanoplatelet thin films. *ACS Nano* **2012**, *6*, 7712-7722.

[92] Wang, X.; Maeda, K.; Thomas, A.; Takanabe, K.;

Xin, G.; Carlsson, J. M.; Domen, K.; Antonietti, M. A metal-free polymeric photocatalyst for hydrogen production from water under visible light. *Nat. Mater.* **2009**, *8*, 76-80.

[93] Chen, S.; Wang, L. W. Thermodynamic oxidation and reduction potentials of photocatalytic semiconductors in aqueous solution. *Chem. Mater.* **2012**, *24*, 3659-3666.

[94] Chen, Y. W.; Prange, J. D.; Dühnen, S.; Park, Y.; Gunji, M.; Chidsey, C. E. D.; McIntyre, P. C. Atomic layer-deposited tunnel oxide stabilizes silicon photoanodes for water oxidation. *Nat. Mater.* **2011**, *10*, 539-544.

[95] Seger, B.; Pedersen, T.; Laursen, A. B.; Vesborg, P. C. K.; Hansen, O.; Chorkendorff, I. Using TiO_2 as a conductive protective layer for photocathodic H_2 evolution. *J. Am. Chem. Soc.* **2013**, *135*, 1057-1064.

[96] Kibsgaard, J.; Chen, Z.; Reinecke, B. N.; Jaramillo, T. F. Engineering the surface structure of MoS_2 to preferentially expose active edge sites for electrocatalysis. *Nat. Mater.* **2012**, *11*, 963-969.

[97] Lukowski, M. A.; Daniel, A. S.; Meng, F.; Forticaux, A.; Li, L.; Jin, S. Enhanced hydrogen evolution catalysis from chemically exfoliated metallic MoS_2 nanosheets. *J. Am. Chem. Soc.* **2013**, *135*, 10274-10277.

[98] Merki, D.; Vrubel, H.; Rovelli, L.; Fierro, S.; Hu, X. Fe, Co, and Ni ions promote the catalytic activity of amorphous molybdenum sulfide films for hydrogen evolution. *Chem. Sci.* **2012**, *3*, 2515-2525.

[99] Popczun, E. J.; McKone, J. R.; Read, C. G.; Biacchi, A. J.; Wiltrout, A. M.; Lewis, N. S.; Schaak, R. E. Nanostructured nickel phosphide as an electrocatalyst for the hydrogen evolution reaction. *J. Am. Chem. Soc.* **2013**, *135*, 9267-9270.

[100] McKone, J. R.; Sadtler, B. F.; Werlang, C. A.; Lewis, N. S.; Gray, H. B. Ni–Mo nanopowders for efficient electrochemical hydrogen evolution. *ACS Catal.* **2013**, *3*, 166-169.

[101] Parsons, R. The rate of electrolytic hydrogen evolution and the heat of adsorption of hydrogen. *Trans. Faraday Soc.* **1958**, *54*, 1053-1063.

[102] Boettcher, S. W.; Warren, E. L.; Putnam, M. C.; Santori, E. A.; Turner-Evans, D.; Kelzenberg, M. D.; Walter, M. G.; McKone, J. R.; Brunschwig, B. S.; Atwater, H. A.; Lewis, N. S. Photoelectrochemical hydrogen evolution using Si microwire arrays. *J. Am. Chem. Soc.* **2011**, *133*, 1216-1219.

[103] Dasgupta, N. P.; Liu, C.; Andrews, S.; Prinz, F. B.; Yang, P. Atomic layer deposition of platinum catalysts on nanowire surfaces for photoelectrochemical water reduction. *J. Am. Chem. Soc.* **2013**, *135*, 12932-12935.

[104] Dai, P.; Xie, J.; Mayer, M. T.; Yang, X.; Zhan, J.; Wang, D. Solar hydrogen generation by silicon nanowires modified with platinum nanoparticle catalysts by atomic layer deposition. *Angew. Chem., Int. Ed.* **2013**, *52*, 11119-11123.

[105] Kye, J.; Shin, M.; Lim, B.; Jang, J. W.; Oh, I.; Hwang, S. Platinum monolayer electrocatalyst on gold nanostructures on silicon for photoelectrochemical hydrogen evolution. *ACS Nano* **2013**, *7*, 6017-6023.

[106] Paracchino, A.; Laporte, V.; Sivula, K.; Grätzel, M.; Thimsen, E. Highly active oxide photocathode for photoelectrochemical water reduction. *Nat. Mater.* **2011**, *10*, 456-461.

[107] Dai, P.; Li, W.; Xie, J.; He, Y.; Thorne, J.; McMahon, G.; Zhan, J.; Wang, D. Forming buried junctions to enhance photovoltage by cuprous oxide in aqueous solutions. *Angew. Chem., Int. Ed.* **2014**, in press, doi: 10.1001/anie.201408375.

[108] Kim, J.; Minegishi, T.; Kobota, J.; Domen, K. Investigation of Cu-Deficient copper gallium selenide thin film as a photocathode for photoelectrochemical water splitting. *Jpn. J. Appl. Phys.* **2012**, *51*, 015802.

[109] Gunawan; Septina, W.; Ikeda, S.; Harada, T.; Minegishi, T.; Domen, K.; Matsumura, M. Platinum and indium sulfide-modified $CuInS_2$ as efficient photocathodes for photoelectrochemical water splitting. *Chem. Commun.* **2014**, *50*, 8941.

[110] Baglio, J. A.; Calabrese, G. S.; Harrison, D. J.; Kamieniecki, E.; Ricco, A. J.; Wrighton, M. S.;

Zoski, G. D. Electrochemical characterization of p-type semiconducting tungsten disulfide photocathodes: efficient photoreduction processes at semiconductor/liquid electrolyte interfaces. *J. Am. Chem. Soc.* **1983**, *105*, 2246-2256.

[111] Hou, Y.; Abrams, B. L.; Vesborg, P. C. K.; Bjorketun, M. E.; Herbst, K.; Bech, L.; Setti, A. M.; Damsgaard, C. D.; Pedersen, T.; Hansen, O.; Rossmeisl, J.; Dahl, S.; Norskov, J. K.; Chorkendorff, I. Bioinspired molecular co-catalysts bonded to a silicon photocathode for solar hydrogen evolution. *Nat. Mater.* **2011**, *10*, 434-438.

[112] Huang, Z.; Chen, Z.; Chen, Z.; Lv, C.; Meng, H.; Zhang, C. $Ni_{12}P_5$ nanoparticles as an efficient catalyst for hydrogen generation via electrolysis and photoelectrolysis. *ACS Nano* **2014**, *8*, 8121-8129.

[113] Warren, E. L.; McKone, J. R.; Atwater, H. A.; Gray, H. B.; Lewis, N. S. Hydrogen-evolution characteristics of Ni-Mo-coated, radial junction, n^+p-silicon microwire array photocathodes. *Energy Environ. Sci.* **2012**, *5*, 9653-9661.

[114] Lin, Y.; Battaglia, C.; Boccard, M.; Hettick, M.; Yu, Z.; Ballif, C.; Ager, J. W.; Javey, A. Amorphous Si thin film based photocathodes with high photovoltage for efficient hydrogen production. *Nano Lett.* **2013**, *13*, 5615-5618.

[115] Huang, Z.; Wang, C.; Chen, Z.; Meng, H.; Lv, C.; Chen, Z.; Han, R.; Zhang, C. Tungsten sulfide enhancing solar-driven hydrogen production from silicon nanowires. *ACS Appl. Mater. & Interfaces* **2014**, *6*, 10408-10414.

[116] Seger, B.; Laursen, A. B.; Vesborg, P. C. K.; Pedersen, T.; Hansen, O.; Dahl, S.; Chorkendorff, I. Hydrogen production using a molybdenum sulfide catalyst on a titanium-protected n^+p-silicon photocathode. *Angew. Chem., Int. Ed.* **2012**, *51*, 9128-9131.

[117] Lin, C. Y.; Lai, Y. H.; Mersch, D.; Reisner, E. Cu_2O|NiO_x nanocomposite as an inexpensive photocathode in photoelectrochemical water splitting. *Chem. Sci.* **2012**, *3*, 3482-3487.

[118] Morales-Guio, C. G.; Tilley, S. D.; Vrubel, H.; Grätzel, M.; Hu, X. Hydrogen evolution from a copper(I) oxide photocathode coated with an amorphous molybdenum sulphide catalyst. *Nat. Commun.* **2014**, *5*, 3059.

[119] Tilley, S. D.; Schreier, M.; Azevedo, J.; Stefik, M.; Graetzel, M. Ruthenium oxide hydrogen evolution catalysis on composite cuprous oxide water-splitting photocathodes. *Adv. Funct. Mater.* **2014**, *24*, 303-311.

[120] Benck, J. D.; Lee, S. C.; Fong, K. D.; Kibsgaard, J.; Sinclair, R.; Jaramillo, T. F. Designing active and stable silicon photocathodes for solar hydrogen production using molybdenum sulfide nanomaterials. *Adv. Energy Mater.* **2014**, in press, 10.1002/aenm.201400739.

[121] Rasiyah, P.; Tseung, A. C. C. The role of the lower metal-oxide higher metal-oxide couple in oxygen evolution reactions. *J. Electrochem. Soc.* **1984**, *131*, 803-808.

[122] Esswein, A. J.; Surendranath, Y.; Reece, S. Y.; Nocera, D. G. Highly active cobalt phosphate and borate based oxygen evolving catalysts operating in neutral and natural waters. *Energy Environ. Sci.* **2011**, *4*, 499-504.

[123] Smith, R. D. L.; Prevot, M. S.; Fagan, R. D.; Zhang, Z.; Sedach, P. A.; Siu, M. K. J.; Trudel, S.; Berlinguette, C. P. Photochemical route for accessing amorphous metal oxide materials for water oxidation catalysis. *Science* **2013**, *340*, 60-63.

[124] Zou, Z. G.; Ye, J. H.; Sayama, K.; Arakawa, H. Direct splitting of water under visible light irradiation with an oxide semiconductor photocatalyst. *Nature* **2001**, *414*, 625-627.

[125] Sun, K.; Pang, X.; Shen, S.; Qian, X.; Cheung, J. S.; Wang, D. Metal oxide composite enabled nanotextured Si photoanode for efficient solar driven water oxidation. *Nano Lett.* **2013**, *13*, 2064-2072.

[126] Hoang, S.; Guo, S.; Hahn, N. T.; Bard, A. J.; Mullins, C. B. Visible light driven photoelectrochemical water oxidation on nitrogen-modified TiO_2 nanowires. *Nano Lett.* **2012**,

12, 26-32.

[127] Diab, M.; Mokari, T. Thermal decomposition approach for the formation of α-Fe_2O_3 mesoporous photoanodes and an α-Fe_2O_3/CoO hybrid structure for enhanced water oxidation. *Inorg. Chem.* **2014**, *53*, 2304-2309.

[128] Lichterman, M. F.; Shaner, M. R.; Handler, S. G.; Brunschwig, B. S.; Gray, H. B.; Lewis, N. S.; Spurgeon, J. M. Enhanced stability and activity for water oxidation in alkaline media with bismuth vanadate photoelectrodes modified with a cobalt oxide catalytic layer produced by atomic layer deposition. *J. Phys. Chem. Lett.* **2013**, *4*, 4188-4191.

[129] Liu, G.; Shi, J.; Zhang, F.; Chen, Z.; Han, J.; Ding, C.; Chen, S.; Wang, Z.; Han, H.; Li, C. A tntalum nitride photoanode modified with a hole-storage layer for highly stable solar water splitting. *Angew. Chem., Int. Ed.* **2014**, *53*, 7295-7299.

[130] Kim, J. Y.; Magesh, G.; Youn, D. H.; Jang, J. W.; Kubota, J.; Domen, K.; Lee, J. S. Single-crystalline, wormlike hematite photoanodes for efficient solar water splitting. *Sci. Rep.* **2013**, *3*, 2681.

[131] Qiu, Y.; Leung, S. F.; Zhang, Q.; Hua, B.; Lin, Q.; Wei, Z.; Tsui, K. H.; Zhang, Y.; Yang, S.; Fan, Z. Efficient photoelectrochemical water splitting with ultrathin films of hematite on three-dimensional nanophotonic structures. *Nano Lett.* **2014**, *14*, 2123-2129.

[132] Li, Y.; Zhang, L.; Torres-Pardo, A.; Gonzalez-Calbet, J. M.; Ma, Y.; Oleynikov, P.; Terasaki, O.; Asahina, S.; Shima, M.; Cha, D.; Zhao, L.; Takanabe, K.; Kubota, J.; Domen, K. Cobalt phosphate-modified barium-doped tantalum nitride nanorod photoanode with 1.5% solar energy conversion efficiency. *Nat. Commun.* **2013**, *4*, 2566.

[133] Abdi, F. F.; Firet, N.; van de Krol, R. Efficient $BiVO_4$ thin film photoanodes modified with cobalt phosphate catalyst and W-doping. *ChemCatChem* **2013**, *5*, 490-496.

[134] Kim, T. W.; Choi, K.-S. Nanoporous $BiVO_4$ photoanodes with dual-layer oxygen evolution catalysts for solar water splitting. *Science* **2014**, *343*, 990-994.

[135] Strandwitz, N. C.; Comstock, D. J.; Grimm, R. L.; Nichols-Nielander, A. C.; Elam, J.; Lewis, N. S. Photoelectrochemical behavior of n-type Si(100) electrodes coated with thin films of manganese oxide grown by atomic layer deposition. *J. Phys. Chem. C* **2013**, *117*, 4931-4936.

[136] Du, C.; Yang, X.; Mayer, M. T.; Hoyt, H.; Xie, J.; McMahon, G.; Bischoping, G.; Wang, D. Hematite-based water splitting with low turn-on voltages. *Angew. Chem., Int. Ed.* **2013**, *52*, 12692-12695.

[137] Chemelewski, W. D.; Lee, H.-C.; Lin, J. F.; Bard, A. J.; Mullins, C. B. Amorphous FeOOH oxygen evolution reaction catalyst for photoelectrochemical water splitting. *J. Am. Chem. Soc.* **2014**, *136*, 2843-2850.

[138] Klepser, B. M.; Bartlett, B. M. Anchoring a molecular iron catalyst to solar-responsive WO_3 improves the rate and selectivity of photoelectrochemical water oxidation. *J. Am. Chem. Soc.* **2014**, *136*, 1694-1697.

[139] Cox, C. R.; Winkler, M. T.; Pijpers, J. J. H.; Buonassisi, T.; Nocera, D. G. Interfaces between water splitting catalysts and buried silicon junctions. *Energy Environ. Sci.* **2013**, *6*, 532-538.

[140] Bard, A. J.; Bocarsly, A. B.; Fan, F. R. F.; Walton, E. G.; Wrighton, M. S. The concept of fermi level pinning at semiconductor-liquid junctions - consequences for energy-conversion efficiency and selection of useful solution redox couples in solar devices. *J. Am. Chem. Soc.* **1980**, *102*, 3671-3677.

[141] Yang, X.; Du, C.; Liu, R.; Xie, J.; Wang, D. Balancing photovoltage generation and charge-transfer enhancement for catalyst-decorated photoelectrochemical water splitting: A case study of the hematite/MnO_x combination. *J. Catal.* **2013**, *304*, 86-91.

[142] Trotochaud, L.; Mills, T. J.; Boettcher, S. W. An optocatalytic model for semiconductor–catalyst water-splitting photoelectrodes based on in situ

optical measurements on operational catalysts. *J. Phys. Chem. Lett.* **2013**, *4*, 931-935.

[143] Mei, B.; Permyakova, A. A.; Frydendal, R.; Bae, D.; Pedersen, T.; Malacrida, P.; Hansen, O.; Stephens, I. E. L.; Vesborg, P. C. K.; Seger, B.; Chorkendorff, I. Iron-Treated NiO as a Highly Transparent p-Type Protection Layer for Efficient Si-Based Photoanodes. *J. Phys. Chem. Lett.* **2014**, *5*, 3456-3461.

[144] Luo, J.; Im, J.-H.; Mayer, M. T.; Schreier, M.; Nazeeruddin, M. K.; Park, N.-G.; Tilley, S. D.; Fan, H. J.; Grätzel, M. Water photolysis at 12.3% efficiency via perovskite photovoltaics and Earth-abundant catalysts. *Science* **2014**, *345*, 1593-1596.

[145] Cox, C. R.; Lee, J. Z.; Nocera, D. G.; Buonassisi, T. Ten-percent solar-to-fuel conversion with nonprecious materials. *Proc. Natl. Acad. Sci. U. S. A.* **2014**, *111*, 14057-14061.